

# Spontaneous immortalization of chicken fibroblasts generates stable, high-yield cell lines for serum-free production of cultured meat

Received: 13 April 2022

Accepted: 3 November 2022

Published online: 22 December 2022

 Check for updates

L. Pasitka<sup>1,5</sup>, M. Cohen<sup>1,2,5</sup>, A. Ehrlich<sup>1</sup>, B. Gildor<sup>3</sup>, E. Reuveni<sup>3</sup>, M. Ayyash<sup>1,3</sup>, G. Wissotsky<sup>3</sup>, A. Herscovici<sup>3</sup>, R. Kaminker<sup>3</sup>, A. Niv<sup>3</sup>, R. Bitcover<sup>3</sup>, O. Dadia<sup>3</sup>, A. Rudik<sup>3</sup>, A. Voloschin<sup>3</sup>, M. Shimoni<sup>3</sup>, Y. Cinnamon<sup>4</sup> & Y. Nahmias<sup>1,2,3</sup>✉

Cellular agriculture could meet growing demand for animal products, but yields are typically low and regulatory bodies restrict genetic modification for cultured meat production. Here we demonstrate the spontaneous immortalization and genetic stability of fibroblasts derived from several chicken breeds. Cell lines were adapted to grow as single-cell suspensions using serum-free culture medium, reaching densities of  $108 \times 10^6$  cells per ml in continuous culture, corresponding to yields of 36% w/v. We show that lecithin activates peroxisome proliferator-activated receptor gamma (PPAR $\gamma$ ), inducing adipogenesis in immortalized fibroblasts. Blending cultured adipocyte-like cells with extruded soy protein, formed chicken strips in which texture was supported by animal and plant proteins while aroma and flavour were driven by cultured animal fat. Visual and sensory analysis graded the product 4.5/5.0, with 85% of participants extremely likely to replace their food choice with this cultured meat product. Immortalization without genetic modification and high-yield manufacturing are critical for the market realization of cultured meat.

Fire grilling of meat was an important step in human evolution<sup>1</sup>. Access to high-density protein allowed our species to increase in numbers, while increased fat availability was associated with encephalization and the development of cultural habits<sup>2–4</sup>. This history of meat consumption left its mark on our emotional responses to the grilling of animal fat as part of a complex interplay between smell, taste and cognition<sup>5</sup>. While meat constitutes only 18% of protein intake worldwide<sup>6</sup>, the demand for animal products is rapidly rising with the urbanization of developing countries<sup>7</sup>. Meeting this increase in demand is challenging as estimates suggest that 14% of global greenhouse emissions are generated by livestock production.

Poultry production is environmentally more efficient than beef and pork<sup>8</sup> but is associated with 25% of foodborne illnesses in the United States, accounting for the highest number of food-related hospitalizations<sup>9</sup>. Antibiotics use in livestock production was also correlated to the development of microbial resistance<sup>10</sup> causing over 35,000 deaths each year in the United States alone. Finally, animal-to-human transmission of highly pathogenic viruses, such as avian influenza and coronavirus, is a major concern<sup>11–13</sup>.

High-throughput production of cultured meat can theoretically reduce greenhouse emissions and increase food safety using a fraction of the environmental resources of traditional agriculture<sup>14</sup>. Primary

<sup>1</sup>Grass Center for Bioengineering, Benin School of Computer Science and Engineering, The Hebrew University of Jerusalem, Jerusalem, Israel.

<sup>2</sup>Department of Cell and Developmental Biology, Silberman Institute of Life Sciences, The Hebrew University of Jerusalem, Jerusalem, Israel. <sup>3</sup>Believer Meats, Rehovot, Israel. <sup>4</sup>Institute of Animal Science, Agricultural Research Organization, The Volcani Center, Bet Dagan, Israel. <sup>5</sup>These authors contributed equally: L. Pasitka, M. Cohen. ✉e-mail: [ynahmias@cse.huji.ac.il](mailto:ynahmias@cse.huji.ac.il)

satellite cells used in the first demonstration of cultured beef can theoretically be expanded up to 800 kg per biopsy, but the process demands a continuous supply of animal tissue<sup>14</sup>. Other groups utilize induced pluripotent stem cells or clustered regularly interspaced short palindromic repeats (CRISPR)-immortalized muscle cells that can proliferate indefinitely<sup>15,16</sup>. However, genetic modification can lead to off-target effects casting doubt on consumer acceptance<sup>17</sup>. One alternative is spontaneous immortalization, a process driven by chromosomal rearrangements and epigenetic changes that occur during repeated cell divisions that characterize fibroblast growth<sup>18</sup>. Fibroblasts replicate fast, have a stable phenotype and require few nutrients for growth, making them an ideal substrate for cultured meat.

Here we demonstrate the spontaneous immortalization of fibroblast lines derived from several chicken breeds and their adaptation to anchorage-independent growth permitting high-density expansion in serum-free medium. Transcriptomic and karyotypic analyses revealed common mechanisms and long-term genetic stability of the immortalized lines. We show that phosphatidylcholine, the major component of soy lecithin, activates peroxisome proliferator-activated receptor gamma (PPAR $\gamma$ ) to drive adipogenesis in immortalized chicken fibroblasts in the absence of hazardous chemicals. Cells were expanded in continuous bioreactors reaching densities of  $108 \times 10^6$  cells per ml. Blending cultured adipocyte-like cells with extruded soy protein formed chicken strips in which texture, aroma and flavour were supported by both animal and plant proteins. A blinded forced-choice study showed a clear 67% preference for cultured chicken. This technology presents a critical stepping stone in the market realization of cultured meat.

## Results

### Spontaneous immortalization of chicken embryonic fibroblasts

Spontaneous immortalization is a low probability event, driven by repeated cell divisions<sup>18</sup>. Primary chicken embryonic fibroblasts (CEF) were isolated from fertilized embryos of broiler Ross 308 and Israeli Baladi chickens (Fig. 1a,b). Cell isolates exhibited elongated, spindle-shaped morphology characteristic of fibroblasts up to 30 days post isolation (Fig. 1b), with doubling time increasing from 25 to 150 hours as cultures progressed (Fig. 1c). Isolated fibroblasts reached crisis around 30 to 70 days post isolation (Fig. 1c,d and Extended Data Fig. 1a), with doubling time of CEF-2 and CEF-4 lines increasing to 504 hours and 462 hours, respectively. Spindle morphology was lost during senescence, with cells increasing in size and accumulating characteristic vacuoles. Breakthrough occurred in 2–5% of isolates, leading to the formation of proliferating colonies (Fig. 1b). Doubling time of these proliferating fibroblasts stabilized at  $20 \pm 2$  hours around 70 days post isolation (Fig. 1d). Cells that passed population doubling 100 were defined as immortalized cell lines and labelled HUN-CF-2 and HUN-CF-4, representing cell lines derived from broiler Ross 308 and Israeli Baladi chickens, respectively (Fig. 1d–f). Both lines proliferated exponentially for over 259 and 466 population doublings (HUN-CF-2 and HUN-CF-4, respectively), showing stable doubling time and morphology in long-term culture (Fig. 1f and Extended Data Fig. 1b). Immunostaining for vimentin, integrin B1, lamin A/C and lamin B1 in

primary (CEF-2) and immortalized (HUN-CF-2) cells showed typical fibroblast characteristics. Stem cell pluripotency markers SOX2 and SSEA-1 were absent in the original population and were not induced by immortalization (Fig. 1g).

To characterize the immortalization events, we compared each primary culture to its corresponding immortalized line and the suspension-adapted clones FMT-SCF-2 and FMT-SCF-4, respectively (Methods). Both immortalization events resulted in the downregulation of the *TP53* expression but little change in *TP53RK* and *TP53I3* (Fig. 1h). *EGFR* and *MYC*, which are often upregulated in human immortalization events<sup>19,20</sup>, were downregulated in both spontaneous events (Fig. 1h and Extended Data Fig. 1c). Despite the changes in *TERT* expression, telomerase activity did not significantly change post-immortalization, suggesting a telomerase-independent mechanism (Fig. 1i).

### Anchorage-independent growth of immortalized fibroblasts

Mesenchymal cells are anchorage-dependent (Fig. 1f) and thus limited by bioreactor surface area resulting in low production yields<sup>21</sup>. To adapt our lines to anchorage-independent growth, we developed a systemic pipeline for the selection of immortalized cells capable of growing as single-cell suspensions (Fig. 2a). Immortalized cells were seeded on AggreWell<sup>TM</sup> plates, forming non-adherent spheroids (Fig. 2a,b). Spheroids were detached and transferred to shaker flasks exposed to increasing agitation (Methods). As shear stress inhibits proliferation of anchorage-dependent cells<sup>22</sup>, this positive selection pressure results in the selection of suspension-adapted clones. Spheroids  $250 \pm 50 \mu\text{m}$  in diameter broke down into aggregates  $50 \pm 20 \mu\text{m}$  in diameter and gradually to single cells over 90 days in culture (Fig. 2b,c). Doubling time decreased from 200 hours during the initial phase to  $20 \pm 2$  hours for both lines following 100 population doublings (Fig. 2c). Suspension-adapted chicken fibroblasts (SCF) exhibiting stable proliferation were named FMT-SCF-2 and FMT-SCF-4 (Fig. 2c).

Serum was previously shown to interfere with the genetic stability of cell lines<sup>23</sup>; therefore, we adapted both FMT-SCF-2 and FMT-SCF-4 to serum-free culture medium (Methods and Fig. 2d). Adapted cells showed rapid expansion in shaker flasks, reaching serum-free densities twofold higher than in serum-supplemented conditions (Extended Data Fig. 2a). Decrease in lamin A/lamin B1 ratio in suspension-adapted compared to primary and immortalized fibroblasts (Fig. 2e and Extended Data Fig. 2b,c) indicated loss of mechanical stress<sup>24,25</sup>.

Master and working cell banks were created for both cell lines (Methods), with samples sent for microbiological and viral assessments (Supplementary Information (Table S1)). Animal species determination was carried out regularly to exclude cell line misidentification (Extended Data Fig. 2d,e). Finally, suspension-grown fibroblasts exhibited a stable phenotype and growth in long-term culture, reaching over 600 population doublings in both FMT-SCF-2 and FMT-SCF-4, representing over 1.5 years of continuous growth (Fig. 2f).

Using RNA-seq analysis, we showed that the immortalized lines clustered together irrespective of breed (Fig. 2g). Comparing each line to their original cell source showed a similar number of differentially expressed genes and 74% overlap between events (Fig. 2h). Enrichment analysis showed that genes involved in extracellular matrix (ECM)–receptor interaction, focal adhesion, DNA replication, homologous

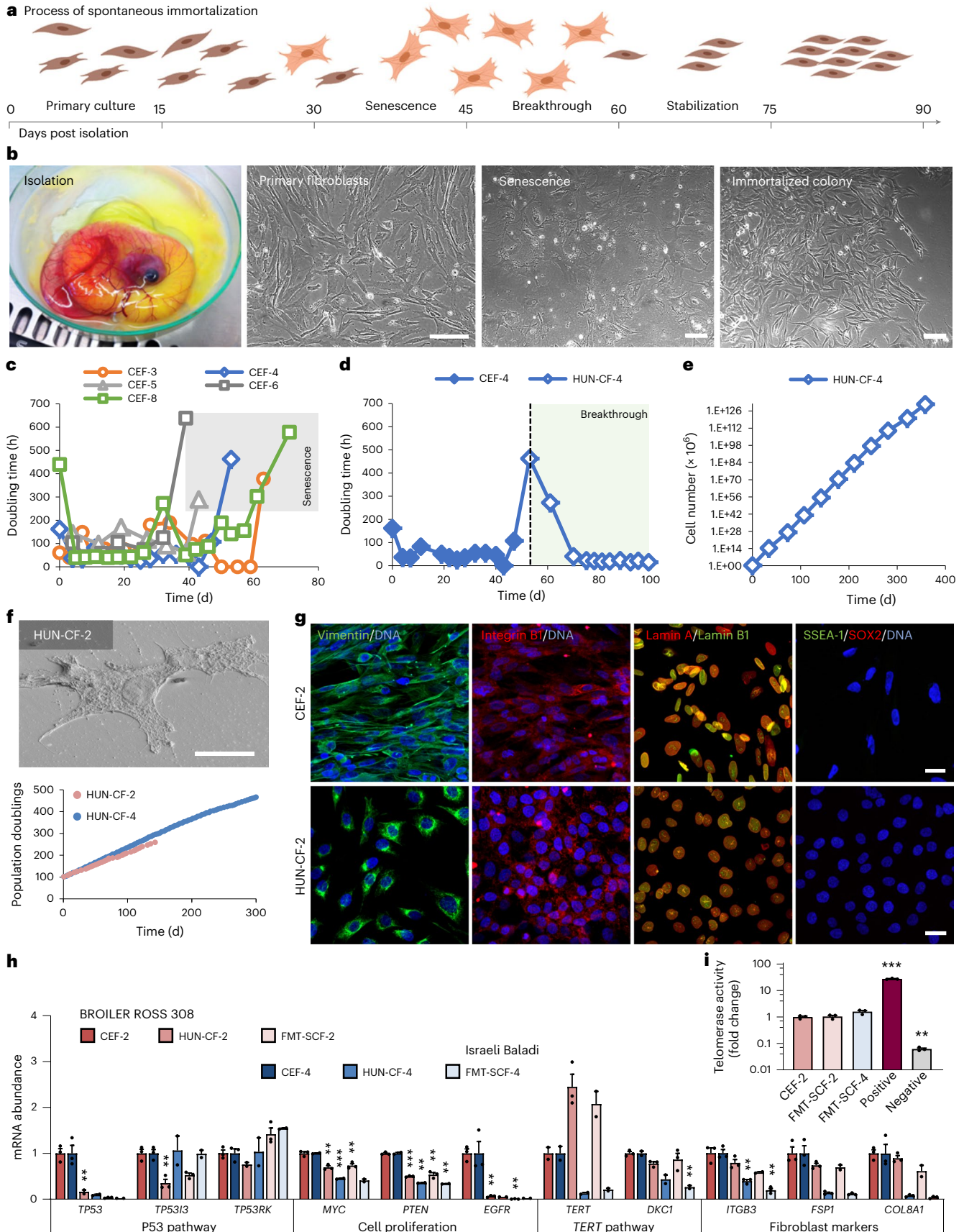
#### Fig. 1 | Spontaneous immortalization of chicken embryonic fibroblasts.

**a**, Schematic diagram depicting the spontaneous immortalization process of fibroblasts. **b**, Phase images of chicken embryonic fibroblasts isolated from fertilized chicken eggs. Scale bars equal  $20 \mu\text{m}$ . **c**, Doubling time of primary cells ranged from 25 to 150 h. Cells entered senescence (grey shading) within 40 to 70 d post isolation. **d**, Breakthrough event (dashed line) in Israeli Baladi chicken (CEF-4). Immortalization occurred within 10 to 30 d after entering senescence. Doubling time stabilized within three weeks to  $20 \pm 2$  h (green shading). **e**, Accumulative cell number of immortalized cells increased exponentially once doubling time stabilized. **f**, HUN-CF-2, visualized by scanning electron

microscope, exhibited stable cell growth for over 300 population doublings. Scale bar equals  $15 \mu\text{m}$ . **g**, Immunostaining of primary and immortalized embryonic fibroblasts from broiler Ross 308 chicken (CEF-2 and HUN-CF-2). Scale bars equal  $20 \mu\text{m}$ . **h**, Gene expression analysis shows downregulation of *TP53* and *EGFR* expression in immortalized cells but little effect on expression levels of *TP53* target genes, *MYC*, *PTEN* or *DKK1* (member of the telomerase reverse transcriptase (TERT) pathway). **i**, Telomerase activity in CEF-2, FMT-SCF-2 and FMT-SCF-4 ( $n = 3$ ). Data in **h** and **i** are presented as means plus standard error of the mean. Student's *t* test *p* values are labelled: \*\* $p < 0.01$ , \*\*\* $p < 0.001$ .

recombination, and cell cycle pathways were differentially expressed following immortalization (Extended Data Fig. 3a,b and Supplementary Table 1 (S1a,b)). These pathways were shared between the two

independent events suggesting common mechanisms (Fig. 2i). Copy number variation analysis of four different cell lines derived from broiler Ross 308 (FMT-SCF-1 and FMT-SCF-2) and Israeli Baladi chicken



(FMT-SCF-3 and FMT-SCF-4) revealed commonality of chromosomal events (Extended Data Fig. 3c,d), further suggesting a common mechanism of spontaneous immortalization.

To characterize cell identity, we performed principal component analysis (PCA) comparing the transcriptome of our cell lines to RNA-seq data reported for other chicken tissues, including kidney, liver, muscle, adipose tissue, gizzard, abdominal fat, satellite cells, chondrocytes and embryonic fibroblasts (Methods, Fig. 2j,k and Extended Data Fig. 3e). Our primary-cell isolates (CEF-2 and CEF-4) clustered together with chicken embryonic fibroblasts, validating our cell source (Fig. 2j,k). Importantly, both immortal cell lines (HUN-CF-2 and HUN-CF-4) and suspension-adapted lines (FMT-SCF-2 and FMT-SCF-4) clustered with chicken primary fibroblasts (CEF-2 and CEF-4). *K*-mean clustering similarly showed that all fibroblast lines cluster together and away from the other tissues (Fig. 2l), suggesting that cell line immortalization did not affect cell identity.

### Genetic stability and safety of immortalized fibroblasts

To study the genetic stability of our anchorage-independent cell lines, we performed RNA-seq and karyotype analysis up to population doubling 536 representing over 400 days of continuous growth (Fig. 3a–c). Chicken macrochromosome number increased from  $18 \pm 1$  in primary cells to  $20 \pm 3$  in immortalized cells primarily due to 1q duplication, but remained stable through population doubling 160 (Fig. 3b,c). Loss of macrochromosomes 6, 7 and 8 observed during early passages of primary chicken fibroblasts became established in both the broiler Ross 308 and Israeli Baladi chicken lines (Fig. 3d).

P53 is the regulator of genomic stability, whose target genes' expression changed minimally during immortalization (Fig. 1h). To rule out P53-driven events, we performed single nucleotide variation (SNV) analysis of *TP53* in FMT-SCF-2 and FMT-SCF-4 and their respective primary chicken fibroblasts. Analysis revealed two SNVs in positions 113 and 402. The variations appear in both the immortal cell lines and the primary chicken isolates and thus are unrelated to the immortalization process (Fig. 3e and Supplementary Table 1 (S1c)). CEF-2 and CEF-4 contain additional SNVs in the *TP53* sequence that were lost in immortalization, possibly due to clonal selection (Supplementary Information (Table S2)). To further demonstrate active DNA repair, we performed a Comet assay on primary chicken fibroblasts and immortalized cells. The data show no significant difference in DNA repair capability between the immortalized and primary fibroblasts (Fig. 3f).

Functional analysis through hidden Markov models (FATHMM) is a method to assess whether variations in genetic data are related to human cancer<sup>26</sup>. We compared the FATHMM scores of FMT-SCF-2 and FMT-SCF-4 to primary chicken fibroblasts that are consumed in a standard diet (Fig. 3g, left). FATHMM distribution was not significantly different between primary chicken cells and the immortalized lines. Mann–Whitney *U* test for events under the  $-0.75$  score threshold was  $p = 0.31$  for broiler Ross 308 and  $p = 0.26$  for Israeli Baladi lines, demonstrating no significant difference between the immortalized lines and commonly consumed cells. The analysis also showed no association with *TP53*-driven cancer mutations (Fig. 3g, right). To further demonstrate lack of tumorigenic potential, we performed a soft agar colony formation assay. Both immortalized lines (FMT-SCF-2

and FMT-SCF-4) failed to form colonies on soft agar, demonstrating that the immortalization events are unassociated with pathogenic transformation (Fig. 3h).

While chickens are not infected with bovine spongiform encephalopathy<sup>27</sup>, we sought to exclude a risk of prion or amyloid diseases. Microscopic analysis (Fig. 2b,f) did not reveal protein aggregates or fibres. Gene expression analysis showed that primary chicken fibroblasts only weakly expressed the prion protein (*PRNP*), and its expression decreased by 50-fold in immortalized cells ( $p < 0.001$ ). Similarly, amyloid beta precursor protein (*APP*), beta-secretase 1 (*BACE1*) and presenilin 1 (*PSEN1*) are not overexpressed by immortalized fibroblasts, suggesting the risk for protein-borne diseases is negligible (Fig. 3i).

### Lecithin-induced adipogenesis of immortalized fibroblasts

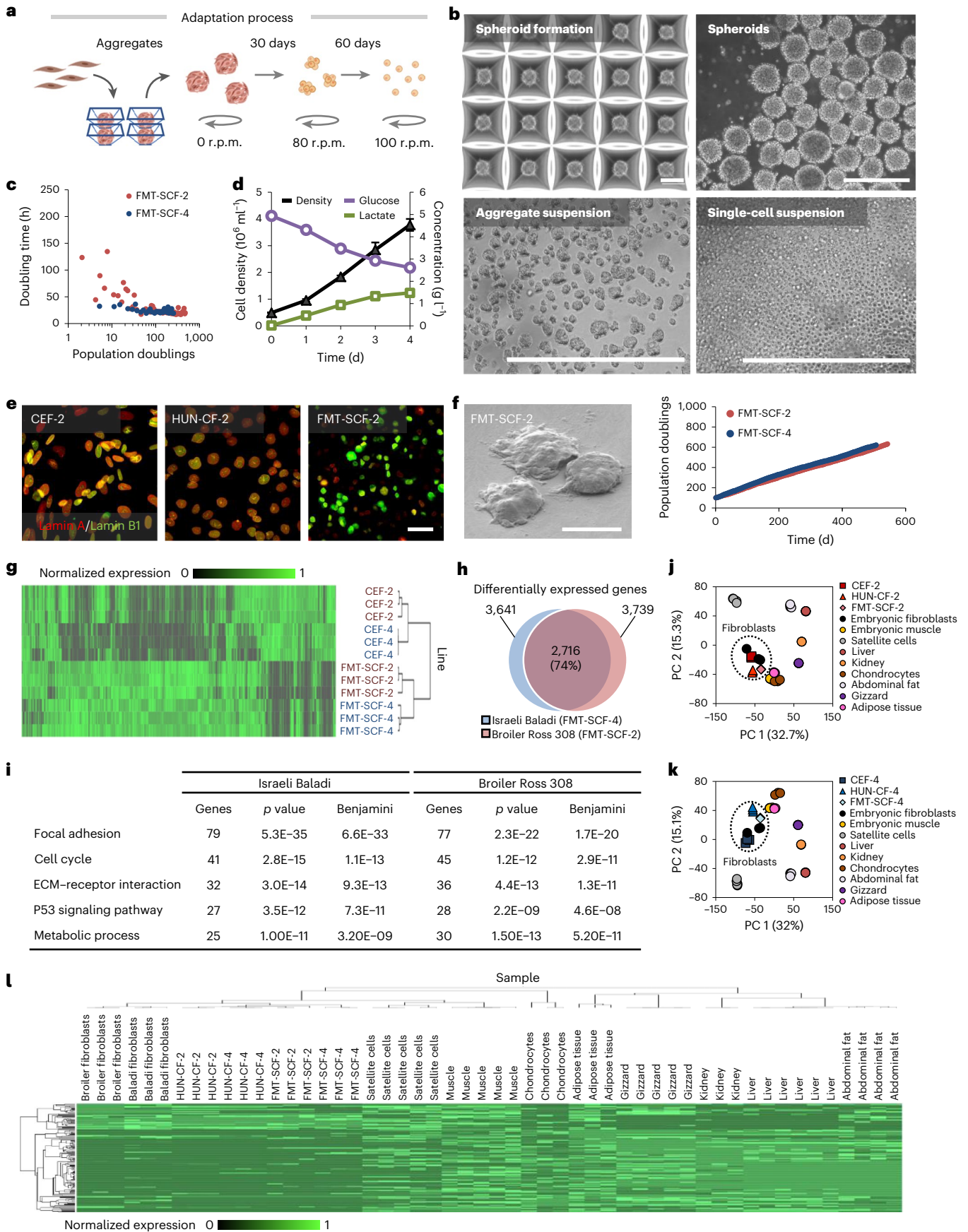
The aroma of meat is derived from the oxidation of fat. Thus, we sought to transdifferentiate our cell lines into adipocyte-like cells. Mammalian adipogenesis is thought to require induction of PPAR $\gamma$  using insulin, corticosteroids and a high dose of 3-isobutyl-1-methylxanthine (IBMX) (Fig. 4a) (ref. 28). As IBMX use in food processes is questionable, we sought to directly activate PPAR $\gamma$ . Adherent HUN-CF-2 and suspension-adapted FMT-SCF-2 cell lines were exposed to rosiglitazone, pristanic acid, and phosphatidylcholine in the presence of 200  $\mu$ M oleic acid (Fig. 4a–d). PPAR $\gamma$  induction resulted in rounder nuclei and adipocyte-like morphology (Fig. 4c and Extended Data Fig. 4a,b). Rosiglitazone, a PPAR $\gamma$ -specific agonist of the thiazolidinedione family<sup>29</sup>, induced intracellular accumulation of lipid droplets in 64% of the population following seven days of exposure (Fig. 4c,d). Pristanic acid, a natural non-specific agonist of PPAR $\alpha/\gamma$ , derived from butter fat, induced a more homogenous accumulation of lipid droplets in 93% of the population, but cellular morphology was mixed (Fig. 4c,d). Phosphatidylcholine is a major component of plant lecithin, previously shown to activate PPAR in mice<sup>30</sup>. Like rosiglitazone, phosphatidylcholine exposure induced a robust accumulation of lipid droplets in 84% of the cells and an adipocyte-like morphology (Fig. 4c,d and Extended Data Fig. 4b). Standard adipogenesis protocol including insulin, dexamethasone, and IBMX (Fig. 4b) failed to induce lipid accumulation or morphological changes in immortalized chicken fibroblasts (Fig. 4c,d). Exposure to oleic acid alone induced some lipid accumulation (Extended Data Fig. 4c–e) but did not result in adipocyte-like morphology (Extended Data Fig. 4c,f).

To confirm the PPAR $\gamma$ -related activity of pristanic acid and phosphatidylcholine, both compounds were tested for activation of peroxisome proliferator response element (PPRE) in a green fluorescent protein (GFP)-reporter cell line (Methods)<sup>31</sup>, with rosiglitazone as a positive control. Rosiglitazone exhibited a strong, 1.8-fold induction ( $p < 0.05$ ) of PPRE activity, while pristanic acid and lecithin showed 1.6- and 2.5-fold induction of PPRE activity over control ( $p < 0.05$ ,  $p < 0.01$ ), respectively (Fig. 4e). Treatment with GW9662, a PPAR $\alpha/\gamma$  inhibitor, inhibited PPRE activation in all conditions (Fig. 4e). Treatment of HUN-CF-2 with rosiglitazone, pristanic acid, or phosphatidylcholine in the presence of GW9662 resulted in inhibition of lipid droplet accumulation and retention of fibroblast spindle morphology, confirming PPAR $\gamma$ -dependent differentiation for all three treatments (Fig. 4f).

### Fig. 2 | Anchorage-independent growth of immortalized chicken fibroblasts in single-cell suspension. a, Schematic depiction of adaptation and selection of clones for single-cell suspensions. b, Phase images of spontaneously immortalized fibroblasts during the adaptation and selection process. Fibroblast spheroids forming in AggreWell™ 400 plates. Scale bars equal 400 $\mu$ m. c, Doubling times tracked during broiler Ross 308 FMT-SCF-2 and Israeli Baladi FMT-SCF-4 selection. d, A maximum cell density of $4.3 \times 10^6$ cells per ml is reached in a serum-free medium-grown batch culture of FMT-SCF-2 after four days ( $n = 3$ ). Data are presented as means plus standard error of the mean. Student's *t* test *p* values are labelled: \* $p < 0.05$ , \*\* $p < 0.01$ , \*\*\* $p < 0.001$ . e, Immunostaining

of primary, immortalized adherent, and suspension-adapted embryonic fibroblasts. Scale bar equals 20  $\mu$ m. f, FMT-SCF-2, visualized by scanning electron microscope, exhibits stable cell growth for over 700 population doublings. Scale bar equals 10  $\mu$ m. g, *K*-mean clustering heatmap of CEF-2 and CEF-4 and FMT-SCF-2 and FMT-SCF-4. h, Venn diagram compares differentially expressed genes between CEF-2 and CEF-4 and FMT-SCF-2 and FMT-SCF-4. i, Enrichment analysis of both lines showed similar terms. j,k, PCA of primary, immortalized adherent, and immortalized suspension lines of broiler Ross 308 (j) and Israeli Baladi (k). l, *K*-mean clustering heatmap comparing primary, immortalized and suspension-adapted cell lines to other tissues.

of primary, immortalized adherent, and suspension-adapted embryonic fibroblasts. Scale bar equals 20  $\mu$ m. f, FMT-SCF-2, visualized by scanning electron microscope, exhibits stable cell growth for over 700 population doublings. Scale bar equals 10  $\mu$ m. g, *K*-mean clustering heatmap of CEF-2 and CEF-4 and FMT-SCF-2 and FMT-SCF-4. h, Venn diagram compares differentially expressed genes between CEF-2 and CEF-4 and FMT-SCF-2 and FMT-SCF-4. i, Enrichment analysis of both lines showed similar terms. j,k, PCA of primary, immortalized adherent, and immortalized suspension lines of broiler Ross 308 (j) and Israeli Baladi (k). l, *K*-mean clustering heatmap comparing primary, immortalized and suspension-adapted cell lines to other tissues.



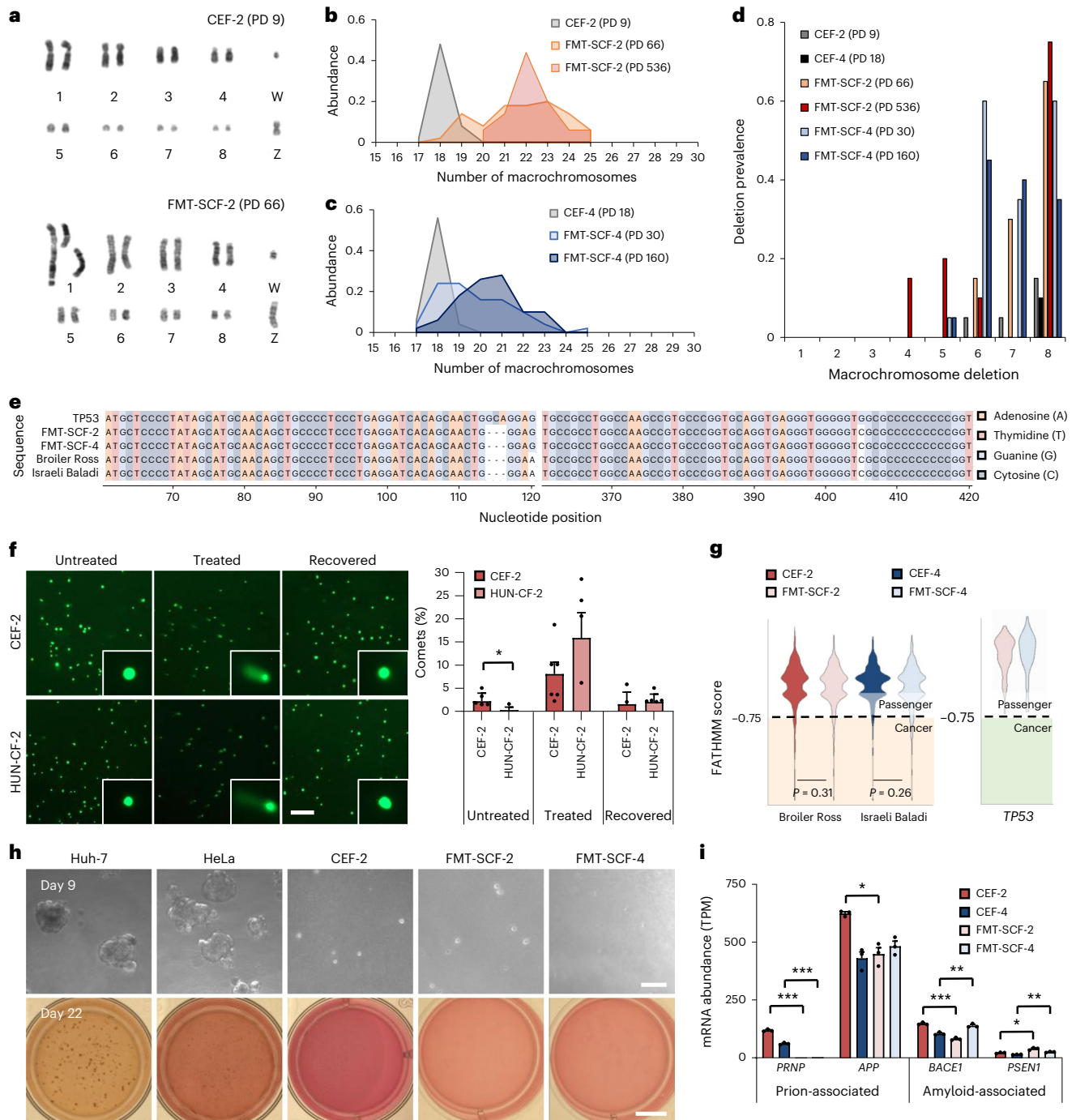


**Fig. 3 | Genetic stability and safety of immortalized chicken fibroblasts.**

**a**, Karyograms displayed no changes in aneuploidy between population doubling (PD) 9 and 66. **b,c**, Chicken karyotype analyses of macrochromosome distribution in FMT-SCF-2 (**b**) and FMT-SCF-4 (**c**) at different PDs. **d**, Macrochromosome deletion in primary fibroblasts and immortalized suspension lines. **e**, SNV analysis of mRNA transcripts of *TP53* in CEF-2, CEF-4, FMT-SCF-2 and FMT-SCF-4. Letters represent DNA bases in different shades (A, adenosine; T, thymidine; G, guanine; C, cytidine). Uncoloured boxes indicate changes from the reference sequence (*TP53*) including base deletions, insertions and point mutations. **f**, Comet assay performed on CEF-2 and HUN-CF-2. Scale bars equal 500  $\mu$ m. **g**, Analysis of human-specific mutations in the chicken transcriptome. Distribution of chicken

genetic regions that correlate to non-synonymous mutations in human genome is not significantly different ( $p > 0.2$ ) between primary chicken cells and the immortalized lines (left). Analysis of the most frequent allele mutations showed no association between these events and common types of human cancer-driving mutations in *TP53* (right). **h**, Soft agar colony formation assay of CEF-2, FMT-SCF-2 and FMT-SCF-4 compared with Huh7 and HeLa cell lines as positive controls. Scale bars equal 100  $\mu$ m (top row) and 10 mm (bottom row). **i**, RNA-seq-based gene expression analysis of prion-disease (*PRNP* and *APP*) and amyloid-disease (*BACE1* and *PSEN1*) associated markers ( $n = 3$ ). Data in graphs in **f** and **i** are presented as means plus standard error of the mean. Student's *t* test  $p$  values are labelled: \*  $p < 0.05$ , \*\*  $p < 0.01$ , \*\*\*  $p < 0.001$ .

Finally, gene expression analysis showed that PPAR $\gamma$  targets such as *ADIPOQ*, *PEPCK1*, *ADRP*, *FABP4*, *PLIN2*, and *CD36* were upregulated in adipogenic induction (Fig. 4g and Extended Data Fig. 4g). These data

demonstrate that adipocyte-like cells can be reliably produced from immortalized suspension-adapted lines using food-grade molecules such as phosphatidylcholine and oleic acid.

### Carrier-free high-density growth of immortalized fibroblasts

The growth of adherent cells is limited by surface area. While carrier beads can be used to grow adherent cells in suspension<sup>21</sup>, maximal cell densities are often limited to  $6\text{--}8 \times 10^6$  cells per ml correlating to a production yield under 2% w/v. We therefore developed a method for carrier bead-free high-density expansion of anchorage-independent chicken cells, seeding anchorage-independent cells in a stirred-tank bioreactor with automated pH and aeration controls (Fig. 5a–d). FMT-SCF-4 cultured in fed-batch reached a viable cell density of  $7 \times 10^6$  cells per ml (Fig. 5a and Extended Data Fig. 5a,b) with daily glucose supplementation (Fig. 5b). However, lactate and ammonium accumulated over time in fed-batch culture reaching concentrations of 7.5 g per l and 0.06 g per l, respectively, thus limiting cell growth (Fig. 5b).

To increase yield, we developed a continuous culture system in which medium was replaced using alternating tangential flow filtration (Fig. 5c–g and Extended Data Fig. 5c,d). Glucose and lactate concentrations were measured and adjusted to maintain a stable metabolic state (Fig. 5d). This perfusion culture reached a viable cell density of  $108 \times 10^6$  cells per ml in 15 days, correlating to a production yield of over 36% w/v or 360 g per l (Fig. 5c–e). The process was robust with three independent runs showing  $\pm 10\%$  variability in outcome (Fig. 5f,g and Extended Data Fig. 5c,d). Fibroblast identity and phenotype were maintained during expansion in bioreactors (Extended Data Fig. 5e,f). Using this high-yield process, cultured chicken adipocyte-like cells were harvested using centrifugation and washed to remove medium residues, producing a pink-white paste (Fig. 5h). Quality control of biomass was performed alongside commercial chicken breast (Extended Data Fig. 6a–f). Minimal pathogen and pesticide residue content in the biomass highlights the safety profile of cultured biomass (Extended Data Fig. 6a).

### Manufacturing of plant/cell hybrid cultured chicken

Animal fat is responsible for the distinct flavour and aroma of meat due to the production of complex polyaromatic hydrocarbons during grilling. In contrast, meat fibrous texture can be mimicked by high-moisture extrusion of plant protein. We therefore developed a method to impregnate chunks of high-moisture extruded soy protein with cultured chicken fat, producing chicken strips that blend plant-based and cell-cultured proteins and fats (Fig. 6a and Supplementary Video S1). Side-by-side comparison of cultured and farmed chicken demonstrated similar fibre cross-section and the distinct Maillard caramelization of meat (Fig. 6b). Nutritional analysis of both products suggested similar nutrition values to farmed chicken (Fig. 6c). Cultured chicken had 22% less saturated fat and 37% less cholesterol than farmed chicken. However, sodium content was higher by 189 mg per 100 g due to the high salt content of texturized soy protein (Fig. 6c).

Preliminary sensory analysis was performed in a non-blinded test (Supplementary Information (Table S3a)). Participants included multiple ethnic backgrounds with 84% identifying as meat eaters and 7% as flexitarians (Fig. 6d). Participants were asked to grade the hybrid chicken product from 0 to 5 on five attributes including overall impression, flavour, texture, aroma, and overall experience; the average score was 4.5 (Fig. 6e). When asked 'how likely are you to replace your meat

choice with this product?', the average likelihood stated by the participants was 8/10 (Fig. 6e).

Next, we performed two independent blinded tastings. In the first study, among 30 participants, 90% identified themselves as meat eaters (Fig. 6f and Supplementary Information (Table S3b)). In blinded, forced-choice tasting, participants compared cultured chicken to its soy base, with identical, minimal seasoning. Sixty-seven percent of the participants preferred cultured chicken over the texturized soy base product (Fig. 6g and Supplementary Information (Table S3b)).

A second blinded sensory tasting analysis was performed to compare cultured chicken and soy base to farmed chicken breast. Participants rated the products as compared to the reference (farmed chicken breast) on texture- and flavour-related attributes (Fig. 6h and Supplementary Information (Table S3c)). The results showed that the addition of cultured adipocyte-like cells improved the rating of most flavour-related attributes, without notably affecting the product texture (Fig. 6h).

## Discussion

Cultured meat production will require either a steady supply of animal biopsies or, more realistically, an immortal cell source. Muscle progenitor cells can be used for cultured meat production<sup>32</sup> but show limited self-renewal<sup>33</sup>. One immortalization approach relies on a combination of CRISPR-Cas9 deletion of tumour suppressors together with *TERT* expression<sup>33,34</sup>. However, while genome editing offers rapid results, it received only limited public acceptance in the United States<sup>35</sup> and is under strict regulatory restrictions in the European Union and China. Recent reports of off-target effects of CRISPR-Cas9 also raise concerns about its application in food<sup>17,36</sup>. Pluripotent stem cells are another potential cell source often considered for cultured meat due to their unlimited replicative capacity. However, phenotypic instability of stem cells and expensive culture media limit their utility<sup>37</sup>. Pluripotent stem cell culture densities are likely limited to  $4.7 \times 10^6$  cells per ml (ref. 38), far below the  $50 \times 10^6$  cells per ml threshold defined for the commercial viability of cultured meat<sup>39</sup>.

Fibroblasts hold an advantage over other cell types due to their stable phenotype and capacity for spontaneous immortalization<sup>18</sup>. Cell lines generated by spontaneous immortalization show phenotypic and karyotypic stability (Figs. 1–3), retaining functional DNA repair capacity (Fig. 3f) even after two years of continuous expansion. Cell lines also do not exhibit a cancer-associated phenotype (Fig. 3).

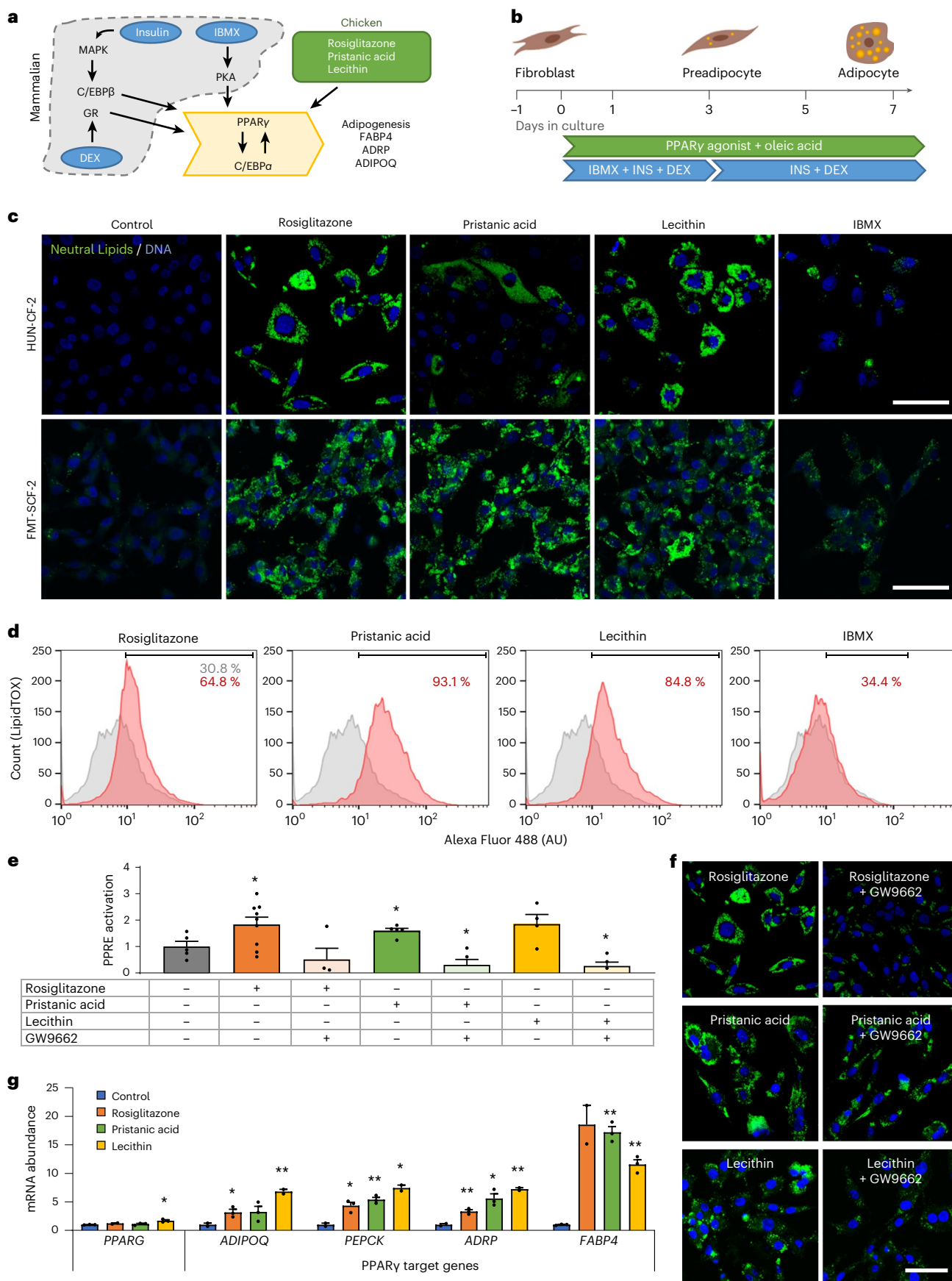
While reaching critical production costs is key, the experience of meat is driven by the distinct aroma and flavour of animal fat<sup>5</sup>. Adipogenesis was thought to be limited to preadipocytes or stem cells and involves the use of IBMX at high concentrations, together with dexamethasone, a regulated pharmaceutical<sup>28,40</sup>. We show that immortalized chicken fibroblasts can be transdifferentiated through direct PPAR $\gamma$  activation (Fig. 4). Use of PPAR $\gamma$  agonists such as pristanic acid<sup>41,42</sup> or L- $\alpha$ -phosphatidylcholine<sup>30</sup> results in the formation of adipocyte-like cells, even in the absence of IBMX (Fig. 4). While pristanic acid is derived from animal products<sup>41</sup>, phosphatidylcholine is found in soybean lecithin and permits the efficient transdifferentiation of over 80% of the cell population.

**Fig. 4 | Transdifferentiation of immortalized fibroblasts to fat-storing adipocyte-like cells.** **a**, Schematic representation of adipogenesis in chicken and mammalian cells. **b**, Schematic diagram of the transdifferentiation process using adipogenic agents. Spindle morphology of fibroblast changes into cuboidal adipocyte morphology, as neutral fats accumulate in lipid droplets. **c**, Confocal images of HUN-CF-2 and FMT-SCF-2 following seven days of transdifferentiation in medium containing rosiglitazone, pristanic acid or soy lecithin with oleic acid, or IBMX. Scale bars equal 50  $\mu\text{m}$ . **d**, Fluorescence activated cell sorting (FACS) analysis revealed homogenous transdifferentiation of over 80% of the population in cells subject to rosiglitazone, pristanic acid and soy lecithin, pink histograms, as compared to control, grey histograms ( $n = 10,000$  cells). AU represents

arbitrary units of fluorescence. Gating is indicated by the line in the top right corner. Percentages represent the part of the population that is considered positive for neutral lipid staining. **e**, Quantification of PPRE activation following 24 h exposure to rosiglitazone, pristanic acid or soy lecithin with oleic acid in the presence or absence of GW9662, a PPAR $\gamma$  inhibitor ( $n = 3$ ). **f**, Confocal images of HUN-CF-2 following seven days of transdifferentiation in medium containing oleic acid and rosiglitazone, pristanic acid or soy lecithin in the presence and absence of PPAR $\gamma$ -inhibitor GW9662. Scale bar equals 50  $\mu\text{m}$ . **g**, Gene expression analysis of the nuclear receptor PPAR $\gamma$  and its target genes ( $n = 3$ ). In all graphs, data are presented as means plus standard error of the mean. Student's *t* test *p* values are labelled: \*  $p < 0.05$ , \*\*  $p < 0.01$ , \*\*\*  $p < 0.001$ .

Scalable manufacturing of adherent cells is a major challenge<sup>43</sup>. Microcarriers can support densities up to  $8 \times 10^6$  cells per ml (ref. 21), far below the maximum of  $214 \times 10^6$  cells per ml reported

for anchorage-free lines such as CHO (ref. 44). We adapted chicken fibroblasts to anchorage-independent growth (Fig. 2), yielding up to  $108 \times 10^6$  cells per ml in perfusion, about 100-fold higher than





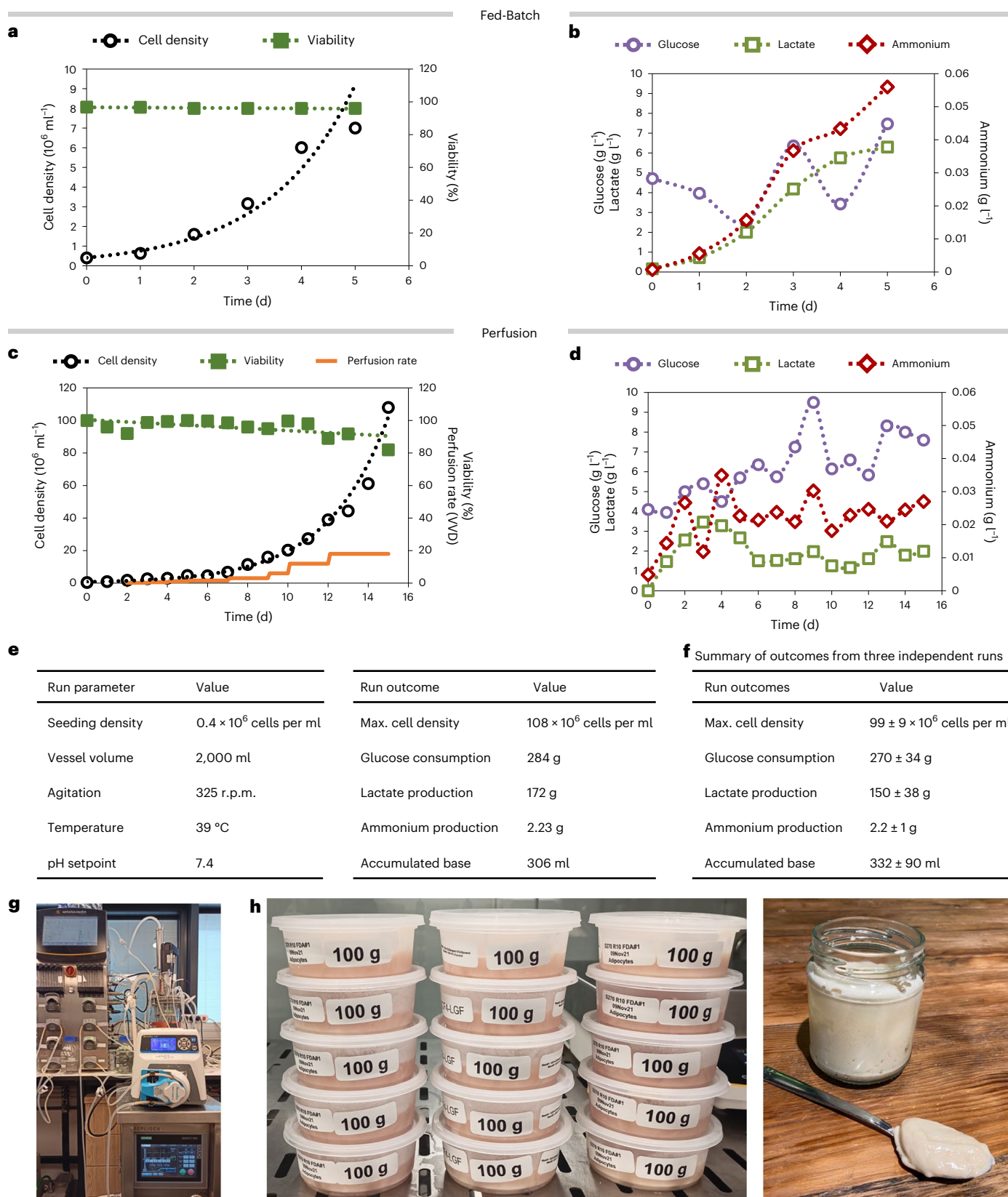


**Fig. 5 | High-density expansion of biomass for cultured chicken meat.**

**a**, Representative fed-batch bioreactor run showing cell density and viability monitored in a five-day culture of FMT-SCF-4. **b**, Accumulation of lactate and ammonium over a five-day fed-batch bioreactor run, while glucose was supplemented daily. **c**, Representative continuously perfused bioreactor run showing cell density, viability, and perfusion rate monitored in a 15-day culture of FMT-SCF-4. Perfusion started on day 2 at 0.1 vessel volumes per day (VVD)

and increased to match cell density through day 15. **d**, Lactate and ammonium concentrations in the perfused bioreactor system. **e**, Perfused bioreactor run parameters (Max., maximal). **f**, Summary of three independent high-density perfusion bioreactor runs. **g**, Photograph of Biostat B System (Sartorius) with a 2 l glass vessel. **h**, Photographs of transdifferentiated biomass as raw material for cultured hybrid chicken product manufacturing.

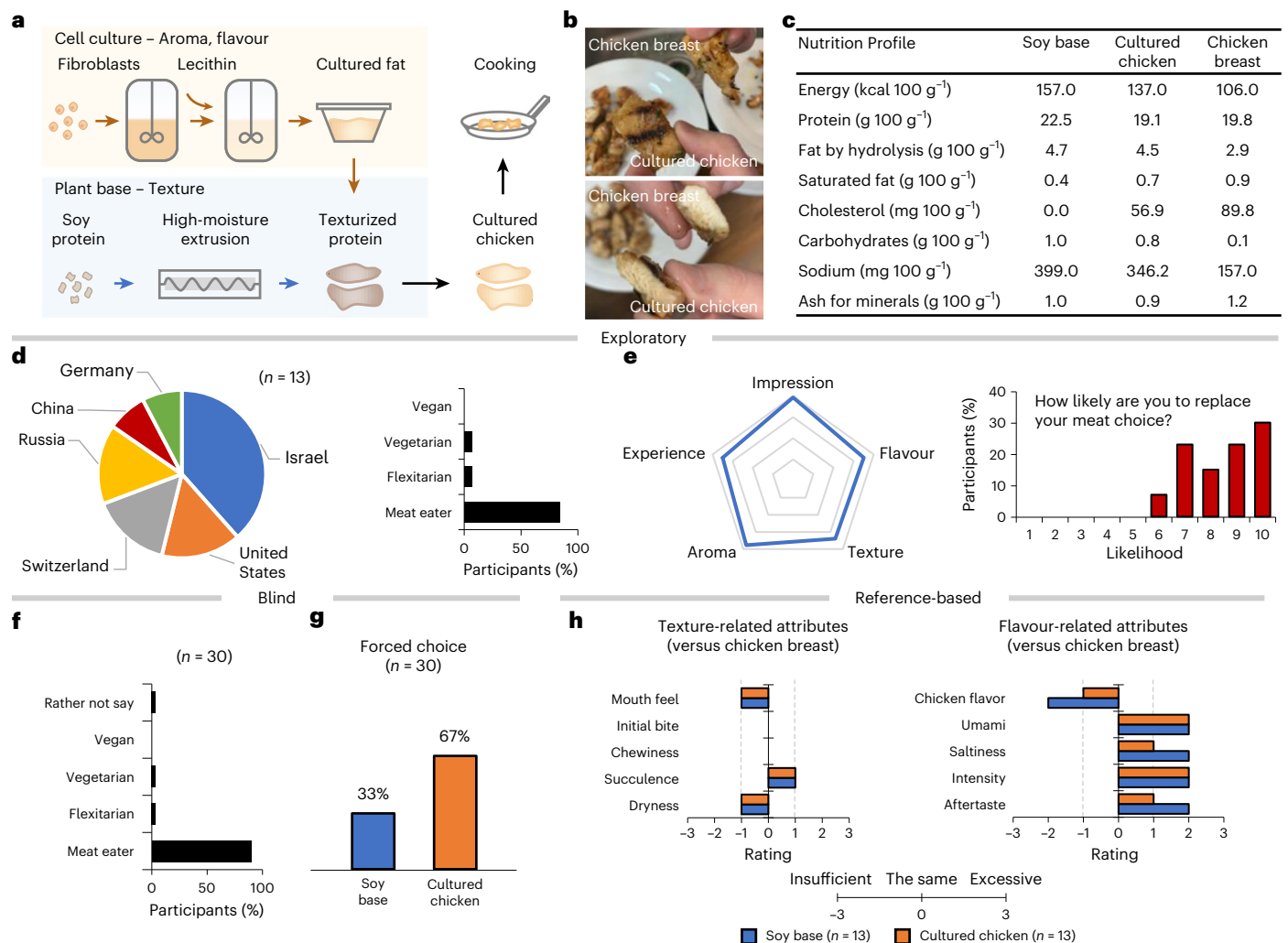


**Fig. 6 | Manufacturing of cultured chicken.** **a**, A schematic depicting the process of production of cultured chicken from the cell to the pan. **b**, Grilled farmed chicken and cultured chicken are indistinguishable by visual comparison. **c**, Nutritional analysis of the soy base and cultured chicken as compared to chicken breast. **d**, Participants of the exploratory tasting trial of the cultured chicken were invited to indicate their nationality and their diet/lifestyle ( $n = 13$ ). **e**, Following grilling and tasting, the participants rated their impression of the cultured chicken and its flavour, texture, aroma, and overall tasting experience and their

wilfulness to replace meat in their diet with such a product ( $n = 13$ ). **f**, In a blinded forced-choice tasting, participants indicated their diet/lifestyle ( $n = 30$ ). **g**, In the forced-choice tasting, 67% of participants preferred the cultured chicken over the texturized soy base product ( $n = 30$ ). **h**, In a blinded reference-based tasting, participants rated sensory attributes of the soy base and the cultured chicken as compared to chicken breast (reference = 0) ( $n = 13$ ). Data in **e** are presented as mean; data in **h** are presented as medians.

standard techniques. This cell density translates to a factory volume that can be 17-fold smaller than microcarrier-based fed-batch systems. Two recent independent analyses suggest that the manufacturing costs of biomass in a large perfusion facility, using similar parameters, would range between US\$ 6 to US\$ 50 per kg, resulting in the cost of hybrid products ranging from US\$ 4 to US\$ 10 per kg, respectively<sup>39</sup>. The cost of chicken breast production was estimated to be US\$ 5.1 to US\$ 8.2 per kg in 2021, thus placing cultured meat in the price range of farmed chicken.

Visual and sensory analyses showed remarkable similarities between cultured and farmed chicken (Fig. 6), while blinded tastings demonstrated a clear preference for cultured chicken over a plant-based product. While this work showed the potential of cultured adipocyte-like cells in meat substitutes, further work must explore the integration of muscle and tendons to provide a more accurate mouth feel. Our work defines a path towards the sustainable production of cultured meat, offering greater food security and safety for coming generations.

## Methods

### Materials

DMEM (01-055-1 A), foetal bovine serum (04-127-1 A), penicillin streptomycin solution (03-031-1B) and L-alanine-L-Glutamine (03-022-1B) were purchased from Biological Industries. Rosiglitazone (R2408), pristanic acid (P6617), soybean L- $\alpha$ -phosphatidylcholine (P7443), WY-14643 (C7081), GW9662 (M6191), oleic acid (W281506), IBMX (I5879), dexamethasone (D2915), Hoechst 33342 (B2261), Hoechst 33258 (B2883), human recombinant insulin (91077 C), KAPA SYBR FAST Universal 2 $\times$  quantitative polymerase chain reaction (qPCR) Master Mix (KK4602), Dulbecco's phosphate-buffered saline (D8662), etoposide (E1383), noble agar (A5431) and pluronic F-68 (P5556) were purchased from Sigma Aldrich. TrypLE express enzyme (#12604054), Opti-MEM (#31985047), GMO extraction kit (4466336), DreamTaq green PCR master mix 2 $\times$  (K1082) and HCS LipidTOX green neutral lipid stain (H34475) and RapidFinder<sup>TM</sup> chicken ID kit (A24393) were purchased from Thermo Fisher Scientific. Paraformaldehyde (00380) was purchased from Polysciences. CAVASOL W6 HP TL was purchased

from Wacker Chemie. qScript cDNA SuperMix was purchased from Quanta BioSciences. RNeasy Mini kit was purchased from Qiagen. AggreWellTM400 plates were purchased from Stem Cell Technologies. COMET assay kit was purchased from Abcam (ab238544). Quick-DNA Miniprep (Zymo Research, D3025) was purchased from Zotal. ScienCell telomerase activity quantification qPCR assay kit (catalogue number 8928) was purchased from Almgog Diagnostic.

### Cell lines

UMNSAH/DF-1 (ATCC CRL-12203), Hep G2 (HEPG2) (ATCC HB-8065), HeLa (CRM-CCL-2) were obtained from the American Type Culture Collection (ATCC). The human hepatoma cell line (Huh7) was obtained from Creative Biolabs. Other cell lines were isolated in this study and described within.

### Isolation of CEF

Freshly laid broiler Ross 308 fertilized eggs were purchased from a commercial breeding farm (Gil Guy Clumeck in Israel), Israeli Baladi fertile eggs were a gift of Mohammad Ghosheh. Chicken eggs were grown in a 38.5 °C humidified incubator for 10–12 d.

Eggs were sprayed with 70% isopropanol, wiped and placed in a sterile dish inside a BSL2 flow hood. Eggs were cracked by gentle tapping and cut with scissors to expose the yolk and the embryo. Inspection revealed a normal embryo with a beating heart. The embryo was released from the yolk, transferred into phosphate buffered salt (PBS) solution and treated according to ethical guidelines. Briefly, the head was removed with a sharp scalpel in a single motion. Next, the limbs, the internal organs and any visible bones were identified and removed. The tissue was washed of any residues of blood with PBS salt solution to follow guidelines of Kosher laws.

The embryo was then transferred into trypsin solution, finely chopped using a scalpel blade and incubated with trypsin in 50 ml tubes at 37 °C for 30 min. Tubes were centrifuged at 100 ×g for 1 min, and 1 ml of the supernatant was seeded in a 75 cm<sup>2</sup> T-flask in DMEM supplemented with 10% (v/v) foetal bovine serum (FBS), 200 units per ml penicillin and streptomycin, and 2 mM L-alanine-L-Glutamine (DMEM10 culture medium). Tubes were then further centrifuged for 5 min at 300 ×g, supernatant was discarded and the pellet resuspended in 5 ml trypsin and incubated at 37 °C for 30 min. All of the supernatant was seeded in 75 cm<sup>2</sup> T-flasks without further centrifugation. Cells were incubated at 39 °C in a humidified incubator under ambient 5% CO<sub>2</sub>; medium was changed daily.

Primary chicken embryonic fibroblast outgrowth produced confluent flasks within 1–2 d. Cells were harvested and cryopreserved to create nine primary-cell banks labelled CEF-1 to 9. Primary fibroblasts were passaged regularly, recording changes in doubling time and morphology as cells underwent senescence (crisis) and breakthrough. Cells were considered immortal once the culture showed stable morphology and doubling time following at least 100 population doublings from isolation. Immortalized lines were expanded and cryopreserved as HUN-CF-1, -2, -4, -5 and -7 in cell banks.

### Suspension culture of immortalized chicken fibroblasts

Fibroblast spheroids were created using AggreWell™400 according to the manufacturer's directions. Briefly,  $1.2 \times 10^6$  spontaneously immortalized fibroblasts were seeded in DMEM10 at a density of 3,867 cells per microwell for 48 h. Spheroids were gently detached and transferred to a low-attachment 10 cm petri dish in culture medium supplemented with 0.1% (v/v) Pluronic F-68. Spheroids were mechanically disturbed daily by vigorous pipetting for four consecutive days. Spheroids were transferred to baffled shaker flasks on day 7 and cultured in a humidified shaker incubator at 39 °C, 5% CO<sub>2</sub> and 80 r.p.m. in DMEM10 culture medium supplemented with 0.1% (v/v) Pluronic F-68. Large cellular aggregates were broken down by TrypLE digestion each week; cells were reseeded at a density of 200,000 cells per ml. Suspension cultures

were counted and diluted back to the initial density 2–3 times a week. Following 30 d of culture, the shaker speed was increased to 100 r.p.m. leading to single-cell suspensions developing for 60 d. Cells were considered anchorage-independent once the culture showed stable doubling time and viability above 94% (Supplementary Information (Table S5)). Anchorage-independent cell lines were expanded and cryopreserved in master-cell banks labelled FMT-SCF-1 to 5 (derived from HUN-CF-1, -2, -5, -4, -7). Working cell banks were prepared for FMT-SCF-2 and FMT-SCF-4 with the lowest doubling times for each breed ( $19 \pm 2$  and  $20 \pm 2$  h, respectively).

Samples of all lines included in the master-cell banks and respective primary cells were tested for avian pathogens at external laboratories (Supplementary Information (Table S1)).

### Growth and metabolic kinetics in serum-free medium

Serum-free UltraCULTURE was used according to the manufacturer's directions. Serum-free medium was composed of DMEM/F12 medium supplemented with 3 µg ml<sup>-1</sup> insulin, 10 ng ml<sup>-1</sup> fibroblast growth factor, 2 µg ml<sup>-1</sup> hydrocortisone, 7 ng ml<sup>-1</sup> sodium selenite, 2 mM L-alanine-L-Glutamine and 10 µg ml<sup>-1</sup> canola lipid mixture. Cells were seeded at a density of 0.3 to 0.5 × 10<sup>6</sup> cells per ml in shaker flasks and cultured at 39 °C in a humidified incubator under ambient 5% CO<sub>2</sub>. Samples were taken daily, centrifuged at 1,300 ×g for 5 min and resuspended in TrypLE solution to break aggregates in the original sample volume. Cell density and viability were measured using Cellaca MX High-throughput Automated Cell Counter (Nexcelom) according to manufacturer's instructions. Glucose and lactate concentrations were measured daily using the BioProfile FLEX2 Automated Cell Culture analyser (Nova Biomedical).

### Transdifferentiation of immortalized fibroblasts to adipocyte-like cells

Immortalized chicken fibroblasts were seeded at  $4 \times 10^3$  cells cm<sup>-2</sup> or  $0.2 \times 10^6$  cells per ml for adherent and suspension cells, respectively. Transdifferentiation medium was composed of DMEM10 containing 200 µM oleic acid alone or oleic acid supplemented with 10 µM rosiglitazone, 50 µM pristanic acid or 12 µg ml<sup>-1</sup> L-α-Phosphatidylcholine (soy lecithin). Transdifferentiation medium was replaced every 2 d for 7 d. Adherent cells were split on day 2 and reseeded back at starting cell density, and suspension-adapted cells were split on day 3 and reseeded at  $0.3 \times 10^6$  cells per ml, respectively. Standard adipogenesis protocol was used as a control with 0.5 mM IBMX, 10 µg ml<sup>-1</sup> insulin and 0.1 µM dexamethasone for 3 d, followed by 10 µg ml<sup>-1</sup> insulin treatment for an additional 4 d. Transdifferentiation efficiency can be calculated using the following equation

$$\text{Transdifferentiation efficiency [fold change]} = \frac{\left( \frac{CD_7}{CD_{3,5}} \right) \times CD_{3,H} \times \frac{L_7}{100}}{CD_0}$$

with CD indicating cell densities on day 0, day 3 or day 7, CD<sub>5</sub> indicating seeding density, CD<sub>H</sub> indicating harvest density and L<sub>7</sub> indicating % of lipid accumulation on day 7 (quantified using fluorescence-activated cell sorting (FACS), Fig. 4d).

### Quantitative RT-PCR

RNA was isolated and purified using RNeasy Mini Kit according to manufacturer's instructions. RNA concentration and purity were determined using NanoDrop ND-1000 spectrophotometer (Thermo Fisher Scientific). cDNA was synthesized from 1 µg RNA sample using qScript cDNA SuperMix according to the manufacturer's protocol. Gene expression analysis was performed using primers as specified in Supplementary Information (Table S4a) and KAPA SYBR FAST Universal 2 × qPCR Master Mix according to manufacturer's directions. Gene transcription was evaluated using the ΔΔCt method normalized to 60S ribosomal protein L32 (RPL32) or ubiquitin C (UBC).

### RNA sequencing (RNA-seq) analysis

RNA was extracted from primary and anchorage-independent cell lines using RNeasy Micro Kit (Qiagen) according to the manufacturer's directions. Library preparation and RNA sequencing were performed by Syntezza Bioscience. Library construction was conducted using a NuGEN TrioRNA-Seq Kit (Tecan) and sequenced on Illumina HiSeqX with paired-end, 150 base pair (bp) reads using the High Output V2 Kit. Sequencing reads were mapped to the University of California Santa Cruz (UCSC) chicken transcriptome (genome build galGal6) using Bowtie2 (22388286), and expression levels of all genes were quantified using RSEM (21816040). RSEM yielded an expression matrix of inferred gene counts. RNA-seq reads for additional cell types were downloaded from Sequence Read Archive (SRA) repository (GSE169291, GSE99146, GSE172606, GSE151450, PRJNA330615, PRJEB12891), along with accompanying metadata. RNA sequence reads were aligned to chicken transcriptome (genome build galGal6) using Spliced Transcripts Alignment to a Reference (STAR)<sup>45</sup>. Normalized reads count, PCA and differential expression analysis was performed using R package DESeq2 (25516281) with default parameters. Reported are *p* values from a negative binomial Wald test. Overall, 3,641 and 3,739 genes showed significant differential mRNA expression between each primary and immortalized chicken cell line with BH-FDR < 0.001 for Israeli Baladi and broiler Ross 308 breeds, respectively. RNA-seq data with accession number GSE169291 are available at National Center for Biotechnology Information, Gene Expression Omnibus (NCBI GEO).

### Processing, analysis, and graphic display of sequencing data

Rstudio (<https://www.rstudio.com/>) was used to perform principal component analysis (PCA; *prcomp* package)<sup>46</sup> and create scatter plots and volcano plots (*ggplot* package)<sup>47</sup>. Hierarchical clustering, heat maps, correlation plots and similarity matrices were created in Morpheus. Gene ontology enrichment analyses and clustering were performed using DAVID Informatics Resources 6.7 (ref. 48). Network maps were created with McGill's Network Analyst Tool using the KEGG database<sup>49</sup>.

### TP53 SNV analysis

SNV analysis in P53 coding regions was performed using RNA-seq of primary (CEF-2 and CEF-4) and suspension-adapted fibroblast lines (FMT-SCF-2 and -4). The reads were aligned to TP53 mRNA (reference genome GRCg7b) using Burrows-Wheeler Alignment algorithm (BWA) (ref. 50), and then the Genome Analysis Toolkit (GATK) pipeline for SNV discovery was used<sup>51</sup>. Results were validated in whole genome sequencing (not shown). A quality threshold of 500 was used in assessing SNVs (Supplementary Table 1 (S1c)).

### Detection of homologous mutations using RNA-seq data

To detect chicken RNA with potential human homology, we used RNA-seq from each chicken sample and aligned it using the *bwa mem*<sup>50</sup> algorithm against a human reference genome (hg38). Mark-Duplicate<sup>52</sup> and haplotypeCaller algorithms were used to identify high-quality SNVs between primary and immortalized lines for each strain separately. SNVs were then classified into synonymous and non-synonymous using ENSEMBL Variant Effect Predictor<sup>53</sup> and human genome draft hg38. Functional predictions were done through hidden Markov models (FATHMM v2.3). Cancer weights (FATHMMcw), frequency of cancer-associated variants from the CanProVar database, wild-type weights, and frequency of neutral polymorphisms from UniRef database were used to determine a FATHMM score. The FATHMM score indicates whether a variant is associated with cancer (prediction CANCER is given for score < -0.75) or neutral (prediction PASSENGER is given for score > -0.75). FATHMM for indels works on indels shorter than 20 bp and emits a prediction (pathogenic or neutral) together with a confidence score (expressed in %).

Isolation of relevant frequent variations was done using MuTect2 (23396013), ANNOVAR (20601685) and FATHMM (24980617)

algorithms, as previously described (30083469)<sup>28</sup>. Briefly, variants were compared with known cancer variants in the NCBI dbSNP database and COSMIC database (25355519). Variants were then screened using MuTect2. Variants were rejected if the confidence, that a mutation is present in the tumour sample (TLOD) score was above 6.3, and if absent from the matched-normal sample (NLOD) score was above 2.2 (*t\_lod\_fstar* filter). For dbSNP variants, a NLOD threshold of 5.5 was used, except if the variant was also present in the COSMIC database. Further filtering was done using homologous mapping event, clustered events, str contraction, alt allele in normal, multi-event alt allele in normal, germline risk and a panel of normals employing default parameters. ANNOVAR (v.2016Feb01) was used to annotate the variants with RefSeq Genes annotations (GRCh38). RefSeq determined the closest gene name or the two closest genes whenever a variant fell within intergenic regions.

### Karyotype analysis

Karyotyping of chicken macrochromosomes was performed by Creative Bioarrays as previously described<sup>54</sup>.

### Analysis of chromosomal rearrangement using whole genome sequencing

Genomic DNA was extracted from FMT-SCF-2 and FMT-SCF-4 using Quick-DNA MicroPrep Zymo-spin IC columns (ZR-D3021, Zymo Research) according to the manufacturer's instructions. DNA was dehydrated on GenTegra DNA tubes and shipped to Syntezza for library preparation. The DNA libraries were sequenced using Illumina's Novaseq S4 cartridge (Novogene). The average coverage was 25× and was uniformly distributed. Whole genome sequence reads were aligned to the chicken reference genome draft (version GRCg6a) using Bowtie2 (22388286) (ref. 55). Segmental copy number variation and aneuploidy were predicted by AneuFinder<sup>56</sup> with default parameters using two size bin lengths of 15 Kbp and 1 Mbp, respectively. Heat maps and dendrograms were plotted using R. DNA-sequencing data with accession number GSE169291 are available at NCBI GEO.

### Telomerase activity

Activity was quantified using the telomerase activity quantification qPCR assay kit. According to manufacturer's instructions, all samples that have a Cq value lower than 33 cycles are considered positive for telomerase activity. The assay was performed on  $5 \times 10^6$  cells of each sample.

### Comet assay

Assay was performed using Comet assay kit (Abcam, ab238544) according to manufacturer's instructions. DNA damage was induced by treating with 50 μM etoposide in DMEM10. Following 1 h of incubation in a cell culture incubator at 39 °C, the etoposide-containing medium was removed and replaced with DMEM10. One of the treated wells per cell type was placed in the incubator for another 5 h for recovery. Control and treated wells without recovery were processed following manufacturer's instructions. Slides were imaged on Zeiss LSM 700.

### Soft agar colony formation assay

Four percent and 8% noble agar in water were autoclaved. To make the lower gel, the 8% agar was cooled to 42 °C in a water bath. DMEM10 was warmed to 37 °C in a water bath. The cooled agar was diluted tenfold in the warmed medium, and 1 ml was dispensed into each well of a 12-well plate. The plate was incubated at 4 °C for 1 h and then prewarmed to 37 °C before seeding.

For seeding, the 4% agar was cooled to 42 °C in a water bath. The cell lines of interest were trypsinized like during passaging. Cells were counted, and single-cell suspensions were prepared in prewarmed DMEM10 to 37 °C. Cells were seeded at a density of  $5 \times 10^4$  cells per well by resuspending  $5 \times 10^4$  cells in 450 μl of prewarmed medium

per well. Cooled 4% agar was diluted tenfold into the cell suspension, mixed well and seeded (0.5 ml per well). Plates were incubated at 4 °C for 15 min; 200 µl of DMEM10 were gently added above the top gel. Cells were incubated at 37 °C (HeLa, Huh7) or 39 °C (CEF-2, FMT-SCF-2, FMT-SCF-4). Medium was topped up as needed. The plates were imaged on day 9 and day 22.

### Species validation by PCR

DNA was extracted from ongoing cultures using the GMO extraction kit according to manufacturer's directions. PCR reaction mix was prepared to final concentrations of 1× DreamTaq green PCR master mix, 500 nM forward primer, 500 nM reverse primer and 1 ng DNA. Primers were obtained from Sigma Aldrich and are specified in Supplementary Information (Table S4b). PCR reactions were performed using a thermocycler.

### RapidFinder species validation

Verification of species DNA was performed using the RapidFinder Chicken ID. DNA was extracted from cell lines of various species common in the meat industry (chicken, bovine, ovine and porcine) using Zymo Research Quick-DNA Miniprep.

### Scanning electron microscopy

Cells were fixed with 4% (v/v) paraformaldehyde for 15 min at room temperature and washed three times with PBS. Fixed cells were pre-coated with an Au–Pd nanolayer using an SC7640 Sputter. Scanning electron microscopy imaging was performed using the FEI Sirion High-Resolution Scanning Electron Microscope (HR SEM). Images were taken at secondary electron detection with an accelerating voltage of 5 kV, a spot size of 4.0 and at a 5.3 mm working distance using high-resolution mode. TSL-EDAX (EDAX) system was mounted for electron back-scattered diffraction.

### Transmission electron microscopy

Cells were seeded in a plastic eight-chamber slide (Lab-Tek), and suspension-cultured cells were centrifuged to form a pellet. Cells were then fixed in 2.5% (v/v) glutaraldehyde, 2% (v/v) paraformaldehyde in 0.1 M cacodylate buffer (pH 7.4) for 5 h at room temperature and incubated at 4 °C overnight. Cells were then rinsed four times, 10 min each in cacodylate buffer and post-fixed and stained with 1% (v/v) osmium tetroxide, 1.5% (v/v) potassium ferricyanide in 0.1 M cacodylate buffer for 1 h. Cells were then washed four times in cacodylate buffer followed by dehydration in increasing concentrations of ethanol (30, 50, 70, 80, 90, and 95% v/v) for 10 min each step followed by three washes in 100% anhydrous ethanol, 20 min each. Following dehydration, the cells were infiltrated with increasing concentrations of Agar 100 resin in ethanol, consisting of 25, 50, 75, and 100% resin for 16 h each. Cells were then embedded in fresh resin and let polymerize in an oven at 60 °C for 48 h. Blocks with embedded cells were sectioned with a diamond knife on an LKB 3 microtome. Ultrathin sections (80 nm) were collected onto 200 mesh, thin bar copper grids. The sections on grids were sequentially stained with uranyl acetate and lead citrate for 10 min each and imaged with Tecnai 12 TEM 100 kV (Phillips) with MegaView II CCD camera.

### Immunofluorescence staining and imaging

Cells were fixed using 4% paraformaldehyde for 15 min at room temperature and washed three times in PBS. Cells were permeabilized in blocking solution (2% (w/v) bovine serum albumin (BSA) and 0.3% (v/v) Triton X-100 in PBS) for 1 h at room temperature followed by an overnight incubation with primary antibodies (Supplementary Information (Table S4c)). Cells were then washed thrice in PBS and incubated with secondary antibodies, diluted in blocking solution for 1 h at room temperature (Supplementary Information (Table S4c)). Following incubation, cells were washed twice in PBS and counterstained with 1 µg ml<sup>-1</sup> Hoechst 33258 for 20 min. Cells were washed once more in PBS

before imaging. Imaging was performed on a Zeiss LSM 700 confocal microscope with solid-state laser lines 405, 488, 555 and 639 nm. Confocal images were taken with C-Apochromat 40× water immersion objective (numerical aperture (NA) 1.8, working distance (WD) 0.28 mm). Analysis was performed using ZEN 2011 Black software (Carl Zeiss).

### Microscopy of lipid accumulation

Lipid staining was performed using HCS LipidTOX neutral lipid stain according to the manufacturer's protocol and counterstained with 1 µg ml<sup>-1</sup> Hoechst 33258. Cells were imaged as described above (immunofluorescence staining and imaging).

### Nuclear eccentricity analysis

Confocal images of HUN-CF-2 control, pristanic acid-, rosiglitazone- and lecithin-treated cells were analysed using a pipeline for detection and analysis of nuclear shape in CellProfiler (Broad Institute).

### Fluorescence-activated cell sorting

Transdifferentiated cells were stained with HCS LipidTOX and 1 µg ml<sup>-1</sup> Hoechst 33258 according to manufacturer's directions. Cells were washed three times and resuspended in FACS buffer containing PBS supplemented with calcium–magnesium ions and 10% (v/v) FBS. FACS analysis was performed in BD Biosciences FACS Aria III cell sorter, and analysis was performed using the FlowJo software (Becton, Dickinson & Company).

### PPAR activation assay

Nuclear receptor reporter library was used as previously described<sup>31</sup>. Briefly, HEPG2 cells expressing destabilized copGFP under the control of multiple PPRE elements were treated with 10 µM of PPAR $\gamma$  agonist rosiglitazone, 50 µM of pristanic acid and 12 µg ml<sup>-1</sup> lecithin in the presence or absence of 10 µM of the PPAR inhibitor GW9662. Following 24 h incubation, cells were counterstained with Hoechst 33342 and imaged using a Zeiss LSM 700 imaging system (Carl Zeiss) with LD Plan Neofluor 20× objective (NA 0.4, WD 7.9 mm). Images were analysed using ZEN 2012 BLUE software (Carl Zeiss). PPRE activation was calculated by normalizing GFP fluorescence to the number of nuclei in each field.

### Fed-batch and high-density perfusion culture

FMT-SCF-4 cells were seeded at densities 0.4 to 0.8 × 10<sup>6</sup> cells per ml in a 2 l glass vessel of the Sartorius Biostat B Twin System with Mass Flow Control System (MFCS) and SCADA data acquisition. Each vessel was equipped with a pitched blade impeller (45°, 3 fins) and a ring-type macro-sparger. pH was set to 7.4 and was controlled using carbon dioxide and sodium bicarbonate. Dissolved oxygen was controlled with a proportional–integral–derivative (PID) controller governed by a thermal mass flow control (TMFC) for each gas (nitrogen, air, oxygen), while the stirring rate of 320 r.p.m. and 325 r.p.m. in fed-batch and perfusion culture, respectively, were kept constant. The temperature set point was 39 °C. Perfusion was performed using the Repligen XCell ATF2 system starting on day 2. Samples were taken manually to measure cell density, cell viability, pH, glucose, lactate and ammonium concentrations on a BioProfile FLEX2 automated cell culture analyser from Nova Biomedical in fed-batch and perfusion cultures (Supplementary Information (Table S5)).

### Preparation of cultured and farmed chicken

FMT-SCF-4 cells were expanded and transdifferentiated with lecithin as described above. Adipocyte-like cells were washed with sterile 2% (v/v) glycerol and stored at –20 °C before use. Microbiological, viral and bacterial assessment (Extended Data Fig. 6) confirmed the cultured fat was clean of contaminants. Cells were mixed with frozen high-moisture extruded pieces of soy protein (soy base) together with soy sauce, agave syrup and tomato powder and vacuum sealed. Nutrient composition was analysed in a certified laboratory (Institute for Food Microbiology

and Consumer Goods Ltd.). Supermarket-purchased farmed chicken breast was marinated similarly. Both cultured and farmed products were prepared using an identical grilling method.

### Product tastings

In the exploratory stage, 13 participants tasted the cultured chicken product in an open format. Participants were presented with the cultured chicken dish during a meal and asked to score their overall impression of the hybrid product and rate its flavour, texture, aroma and overall experience. Rating was performed with a pencil and paper questionnaire (Supplementary Information (Table S3a)). Attributes ranked from 1 to 5 including impression, flavour, texture, aroma and overall experience. Participants were also asked how likely they are to agree to replace their meat with this type of product (1–10, unlikely to very likely). Finally, the participants were invited to indicate their age, gender, nationality and their diet/lifestyle (vegan, vegetarian, flexitarian, meat eater).

Next, in a blinded tasting, 30 participants tasted the cultured chicken product side by side with the soy base and were asked to rate both products according to various texture- and flavour-related attributes on a scale of 0 to 20 (0—too mild/dislike, 10—just right, 20—too strong/like; Supplementary Information (Table S3b)). Participants were also asked to choose one product as a preference (forced choice). Finally, the participants were invited to indicate their diet/lifestyle.

In a blinded side-by-side tasting, 13 participants tasted the hybrid cultured chicken product and the soy base as compared to the reference of farm-raised chicken breast (reference-based tasting). Participants were asked to rate the general flavour, texture, aroma and overall experience and more specific comparative attributes of flavour, texture, and appearance and were invited to expose which of the products tasted they preferred. Rating was performed with a pencil and paper questionnaire (Supplementary Information (Table S3c)).

### Statistical analysis

Experiments were repeated two or three times with duplicate or triplicate samples for each experimental condition unless stated otherwise. Data from representative experiments are presented, and similar trends were seen in multiple trials. A parametric two-tailed Student's *t* test was used for calculating significant differences between groups. All error bars represent plus standard error of the mean unless otherwise noted. One asterisk indicates  $p \leq 0.05$ , two asterisks indicate  $p \leq 0.01$  and three asterisks indicate  $p \leq 0.001$ .

### Ethical approvals

All protocols involving chicken embryos were reviewed and exempted by the Hebrew University of Jerusalem Institutional Animal Care and Use Committee.

Product tasting was performed following the approval of the Hebrew University of Jerusalem Institutional Review Board (number 13092021). All participants provided written informed consent signed by the participant or legally authorized representative.

### Reporting summary

Further information on research design is available in the Nature Portfolio Reporting Summary linked to this article.

### Data availability

Sequencing data are available at NCBI GEO. The GEO accession number is GSE169291. All data generated or analysed during this study are included in this published article (and its supplementary information files). Source data are provided with this paper.

### Code availability

Our custom Single Cell Analysis CellProfiler Pipeline is available at <https://github.com/Avnere/Single-Cell-Analysis-CellProfiler-Pipeline>.

## References

- Pereira, P. M. & Vicente, A. F. Meat nutritional composition and nutritive role in the human diet. *Meat Sci.* **93**, 586–592 (2013).
- Aiello, L. C. & Wheeler, P. The expensive-tissue hypothesis. *Curr. Anthropol.* **36**, 199–221 (1995).
- Williams, A. C. & Hill, L. J. Meat and nicotinamide: a causal role in human evolution, history, and demographics. *Int. J. Tryptophan Res.* **10**, 1178646917704661 (2017).
- Leonard, W.R., Snodgrass, J.J. & Robertson, M.L. in *Fat Detection: Taste, Texture, and Post Ingestive Effects* (eds Montmayeur, J.-P. & Johannes le Coutre, J.) Ch. 1 (CRC Press/Taylor & Francis, 2010).
- Shepherd, G. M. Smell images and the flavour system in the human brain. *Nature* **444**, 316–321 (2006).
- Henchion, M., Hayes, M., Mullen, A. M., Fenelon, M. & Tiwari, B. Future protein supply and demand: strategies and factors influencing a sustainable equilibrium. *Foods* **6**, 53–74 (2017).
- Alexandratos, N. & Bruinsma, J. *World Agriculture Towards 2030/2050: The 2012 Revision* ESA Working Paper No. 12-03 (FAO, 2012).
- de Vries, M. & de Boer, I. J. M. Comparing environmental impacts for livestock products: a review of life cycle assessments. *Livest. Sci.* **128**, 1–11 (2010).
- Chai, S. J., Cole, D., Nisler, A. & Mahon, B. E. Poultry: the most common food in outbreaks with known pathogens, United States, 1998–2012. *Epidemiol. Infect.* **145**, 316–325 (2017).
- Mathew, A. G., Cissell, R. & Liamthong, S. Antibiotic resistance in bacteria associated with food animals: a United States perspective of livestock production. *Foodborne Pathog. Dis.* **4**, 115–133 (2007).
- de Jong, M. D. & Hien, T. T. Avian influenza A (H5N1). *J. Clin. Virol.* **35**, 2–13 (2006).
- Wong, S. S. & Yuen, K. Y. Avian influenza virus infections in humans. *Chest* **129**, 156–168 (2006).
- Chen, S., Zhang, L., Wang, L., Ouyang, H. & Ren, L. Viruses from poultry and livestock pose continuous threats to human beings. *Proc. Natl Acad. Sci. USA* **118**, e2022344118 (2021).
- Post, M. J. et al. Scientific, sustainability and regulatory challenges of cultured meat. *Nat. Food* **1**, 403–415 (2020).
- Genovese, N. J., Domeier, T. L., Telugu, B. P. & Roberts, R. M. Enhanced development of skeletal myotubes from porcine induced pluripotent stem cells. *Sci. Rep.* **7**, 41833 (2017).
- Ben-Arye, T. et al. Textured soy protein scaffolds enable the generation of three-dimensional bovine skeletal muscle tissue for cell-based meat. *Nat. Food* **1**, 210–220 (2020).
- Fu, Y. et al. High-frequency off-target mutagenesis induced by CRISPR-Cas nucleases in human cells. *Nat. Biotechnol.* **31**, 822–826 (2013).
- Fridman, A. L. & Tainsky, M. A. Critical pathways in cellular senescence and immortalization revealed by gene expression profiling. *Oncogene* **27**, 5975–5987 (2008).
- Pires, M. M., Hopkins, B. D., Saal, L. H. & Parsons, R. E. Alterations of EGFR, P53 and PTEN that mimic changes found in basal-like breast cancer promote transformation of human mammary epithelial cells. *Cancer Biol. Ther.* **14**, 246–253 (2013).
- Kim, J., Eltoum, I. E., Roh, M., Wang, J. & Abdulkadir, S. A. Interactions between cells with distinct mutations in c-MYC and Pten in prostate cancer. *PLoS Genet.* **5**, e1000542 (2009).
- Verbruggen, S., Luining, D., van Essen, A. & Post, M. J. Bovine myoblast cell production in a microcarriers-based system. *Cytotechnology* **70**, 503–512 (2018).
- Luo, W. et al. Lamina shear stress delivers cell cycle arrest and anti-apoptosis to mesenchymal stem cells. *Acta Biochim. Biophys. Sin.* **43**, 210–216 (2011).

23. Wazer, D. E. et al. Loss of P53 protein during radiation transformation of primary human mammary epithelial cells. *Mol. Cell. Biol.* **14**, 2468–2478 (1994).
24. Buxboim, A. et al. Matrix elasticity regulates lamin-A,C phosphorylation and turnover with feedback to actomyosin. *Curr. Biol.* **24**, 1909–1917 (2014).
25. Swift, J. et al. Nuclear lamin-A scales with tissue stiffness and enhances matrix-directed differentiation. *Science* **341**, 1240104 (2013).
26. Shihab, H. A., Gough, J., Cooper, D. N., Day, I. N. & Gaunt, T. R. Predicting the functional consequences of cancer-associated amino acid substitutions. *Bioinformatics* **29**, 1504–1510 (2013).
27. Moore, J. et al. Studies of the transmissibility of the agent of bovine spongiform encephalopathy to the domestic chicken. *BMC Res. Notes* **4**, 501 (2011).
28. Reed, B. C. & Lane, M. D. Insulin receptor synthesis and turnover in differentiating 3T3–L1 preadipocytes. *Proc. Natl Acad. Sci. USA* **77**, 285–289 (1980).
29. Lehmann, J. M. et al. An antidiabetic thiazolidinedione is a high affinity ligand for peroxisome proliferator-activated receptor gamma (PPAR gamma). *J. Biol. Chem.* **270**, 12953–12956 (1995).
30. Zhang, Y., Huang, C., Sheng, X., Gong, Z. & Zang, Y. Q. Lecithin promotes adipocyte differentiation and hepatic lipid accumulation. *Int. J. Mol. Med.* **23**, 449–454 (2009).
31. Levy, G. et al. Nuclear receptors control pro-viral and antiviral metabolic responses to hepatitis C virus infection. *Nat. Chem. Biol.* **12**, 1037–1045 (2016).
32. Post, M. J. Cultured beef: medical technology to produce food. *J. Sci. Food Agric.* **94**, 1039–1041 (2014).
33. Genovese, N., Desmet, D. & Schulze, E. Compositions and methods for increasing the efficiency of cell cultures used for food production. US patent EP3638777A4 (2019).
34. Zhao, Z. et al. Immortalization of human primary prostate epithelial cells via CRISPR inactivation of the CDKN2A locus and expression of telomerase. *Prostate Cancer Prostatic Dis.* **24**, 233–243 (2021).
35. Shew, A. M., Nalley, L. L., Snell, H. A., Nayga, R. M. & Dixon, B. L. CRISPR versus GMOs: public acceptance and valuation. *Glob. Food Secur.* **19**, 71–80 (2018).
36. Lin, Y. et al. CRISPR/Cas9 systems have off-target activity with insertions or deletions between target DNA and guide RNA sequences. *Nucleic Acids Res.* **42**, 7473–7485 (2014).
37. Henry, M. P., Hawkins, J. R., Boyle, J. & Bridger, J. M. The genomic health of human pluripotent stem cells: genomic instability and the consequences on nuclear organization. *Front. Genet.* **9**, 623 (2018).
38. Abecasis, B. et al. Expansion of 3D human induced pluripotent stem cell aggregates in bioreactors: bioprocess intensification and scaling-up approaches. *J. Biotechnol.* **246**, 81–93 (2017).
39. Humbird, D. Scale-up economics for cultured meat: techno-economic analysis and due diligence (2020).
40. Pu, Y. & Veiga-Lopez, A. PPAR $\gamma$  agonist through the terminal differentiation phase is essential for adipogenic differentiation of fetal ovine preadipocytes. *Cell. Mol. Biol. Lett.* **22**, 6 (2017).
41. Zomer, A. W. et al. Pristanic acid and phytanic acid: naturally occurring ligands for the nuclear receptor peroxisome proliferator-activated receptor alpha. *J. Lipid Res.* **41**, 1801–1807 (2000).
42. Mehta, F., Theunissen, R. & Post, M. J. Adipogenesis from bovine precursors. *Methods Mol. Biol.* **1889**, 111–125 (2019).
43. Stephens, N. et al. Bringing cultured meat to market: technical, socio-political, and regulatory challenges in cellular agriculture. *Trends Food Sci. Technol.* **78**, 155–166 (2018).
44. Clincke, M. F. et al. Very high density of CHO cells in perfusion by ATF or TFF in WAVE bioreactor. Part I. Effect of the cell density on the process. *Biotechnol. Prog.* **29**, 754–767 (2013).
45. Dobin, A. et al. STAR: ultrafast universal RNA-seq aligner. *Bioinformatics* **29**, 15–21 (2013).
46. Sigg, C. D. & Buhmann, J. M. Expectation-maximization for sparse and non-negative PCA. In *Proc. 25th International Conference on Machine Learning* 960–967 (Association for Computing Machinery, 2008).
47. Wickham, H. in *ggplot2: Elegant Graphics for Data Analysis* (eds Gentleman, R., Hornik K., & Parmigiani, G.) 241–253 (Springer International Publishing, 2016).
48. Huang, D. W., Sherman, B. T. & Lempicki, R. A. Systematic and integrative analysis of large gene lists using DAVID bioinformatics resources. *Nat. Protoc.* **4**, 44–57 (2009).
49. Xia, J., Gill, E. E. & Hancock, R. E. W. NetworkAnalyst for statistical, visual and network-based meta-analysis of gene expression data. *Nat. Protoc.* **10**, 823–844 (2015).
50. Li, H. & Durbin, R. Fast and accurate short read alignment with Burrows–Wheeler transform. *Bioinformatics* **25**, 1754–1760 (2009).
51. Brouard, J. S., Schenkel, F., Marete, A. & Bissonnette, N. The GATK joint genotyping workflow is appropriate for calling variants in RNA-seq experiments. *J. Anim. Sci. Biotechnol.* **10**, 44 (2019).
52. Van der Auwera, G. A. et al. From FastQ data to high confidence variant calls: the Genome Analysis Toolkit best practices pipeline. *Curr. Protoc. Bioinformatics* **43**, 110.11–110.33 (2013).
53. Naithani, S., Geniza, M. & Jaiswal, P. Variant effect prediction analysis using resources available at Gramene database. *Methods Mol. Biol.* **1533**, 279–297 (2017).
54. Yoshida, M. C., Ikeuchi, T. & Sasaki, M. Differential staining of parental chromosomes in interspecific cell hybrids with a combined quinacrine and 33258 Hoechst technique. *Proc. Japan Acad.* **51**, 184–187 (1975).
55. Langmead, B. & Salzberg, S. L. Fast gapped-read alignment with Bowtie 2. *Nat. Methods* **9**, 357–359 (2012).
56. Bakker, B. et al. Single-cell sequencing reveals karyotype heterogeneity in murine and human malignancies. *Genome Biol.* **17**, 115 (2016).

## Acknowledgements

We thank the Sam and Rina Frankel Foundation (donation; Y.N.) and Believer Meats (Y.N.) for funding this work. Further, we thank D. Petrova, R. Barak, H. Zukerman Narodizky, L. Shirony, A. Nagawkar and M. Rosenberg for technical support.

## Author contributions

Conceptualization and funding by Y.N. Investigation by L.P., M.C., M.S., M.A., G.W. and B.G. Methodology by Y.N., M.C., L.P., A.E., G.W., A.N., A.H., A.R., R.K., R.B., O.D. and A.V. Resources by Y.C. Software by A.E. and E.R. Writing by Y.N., L.P., M.C. and A.E.

## Competing interests

Y.N. is the chief scientific officer, director and shareholder in Believer Meats. M.A., G.W., B.G., E.R., A.H., A.R., R.K., R.B., O.D., A.V. and M.S. are employees of Believer Meats. M.C. is a consultant of Believer Meats. L.P., A.E., A.N. and Y.C. declare no competing interests.

## Additional information

**Extended data** is available for this paper at <https://doi.org/10.1038/s43016-022-00658-w>.

**Supplementary information** The online version contains supplementary material available at <https://doi.org/10.1038/s43016-022-00658-w>.

**Correspondence and requests for materials** should be addressed to Y. Nahmias.

**Peer review information** *Nature Food* thanks Min Du and the other, anonymous, reviewer(s) for their contribution to the peer review of this work.

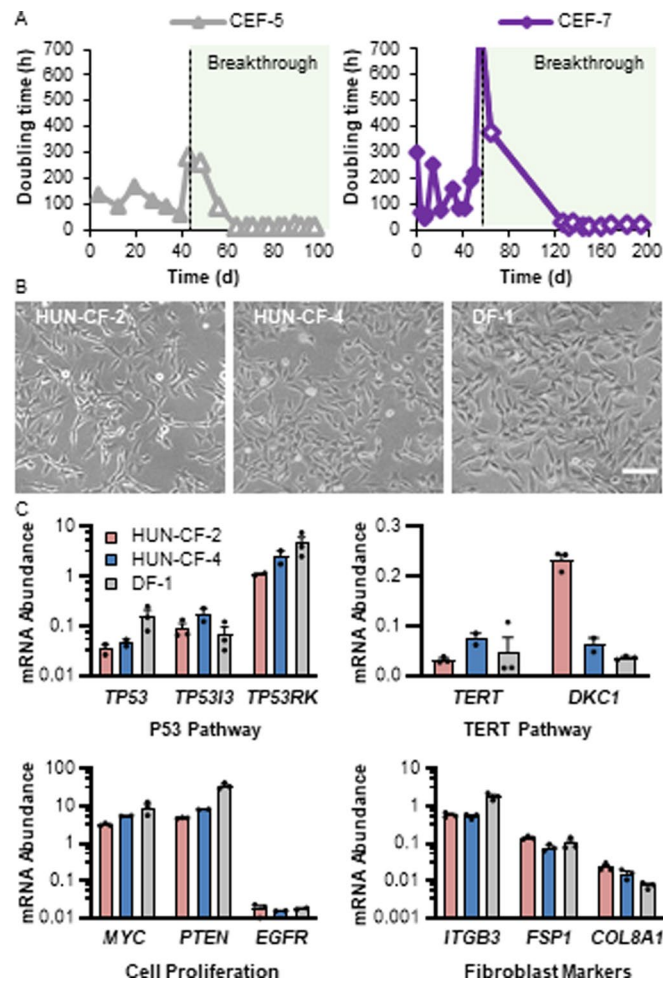
**Reprints and permissions information** is available at [www.nature.com/reprints](http://www.nature.com/reprints).

**Publisher's note** Springer Nature remains neutral with regard to jurisdictional claims in published maps and institutional affiliations.

Springer Nature or its licensor (e.g. a society or other partner) holds exclusive rights to this article under a publishing agreement with the author(s) or other rightsholder(s); author self-archiving of the accepted manuscript version of this article is solely governed by the terms of such publishing agreement and applicable law.

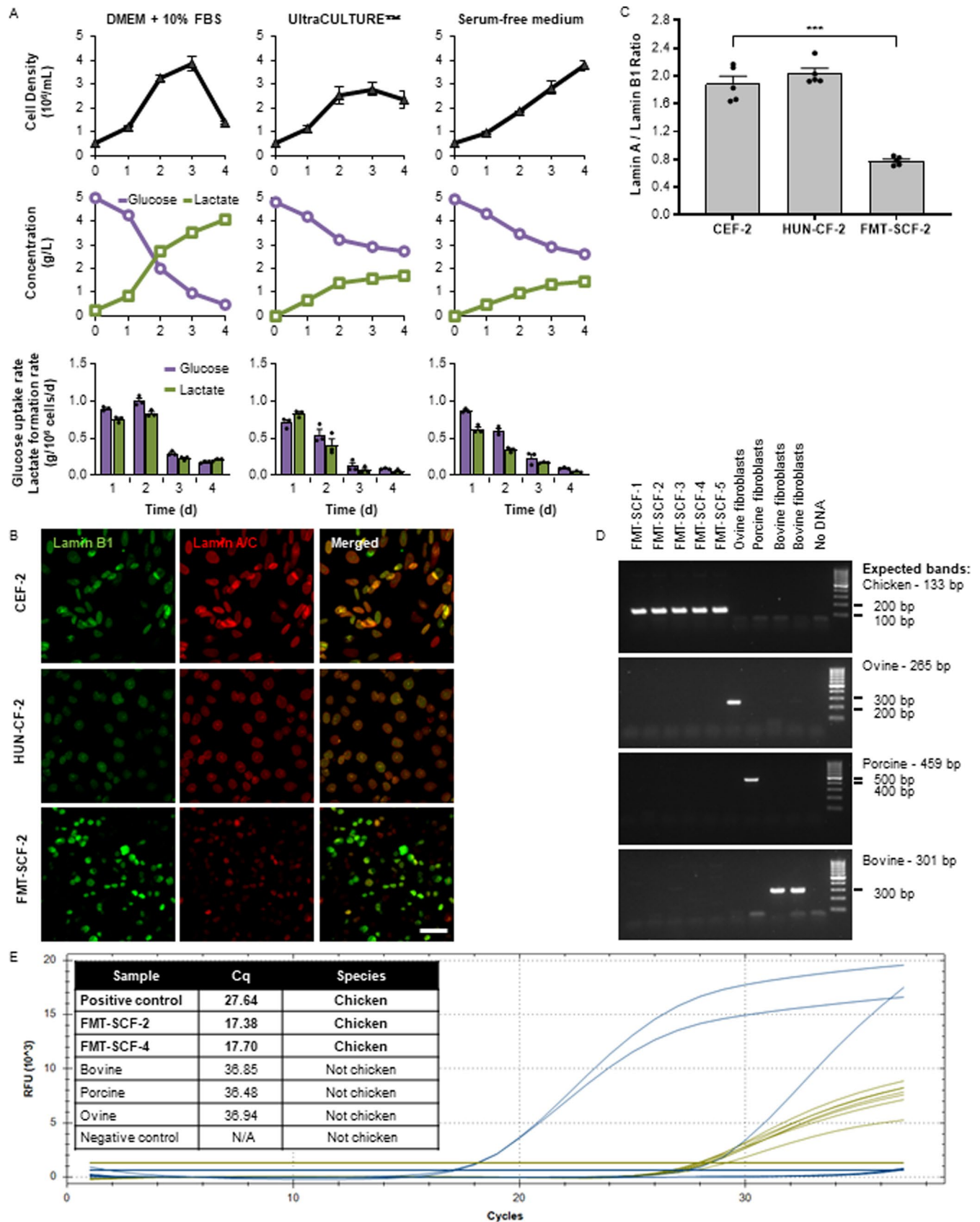
© The Author(s), under exclusive licence to Springer Nature Limited 2022, corrected publication 2023





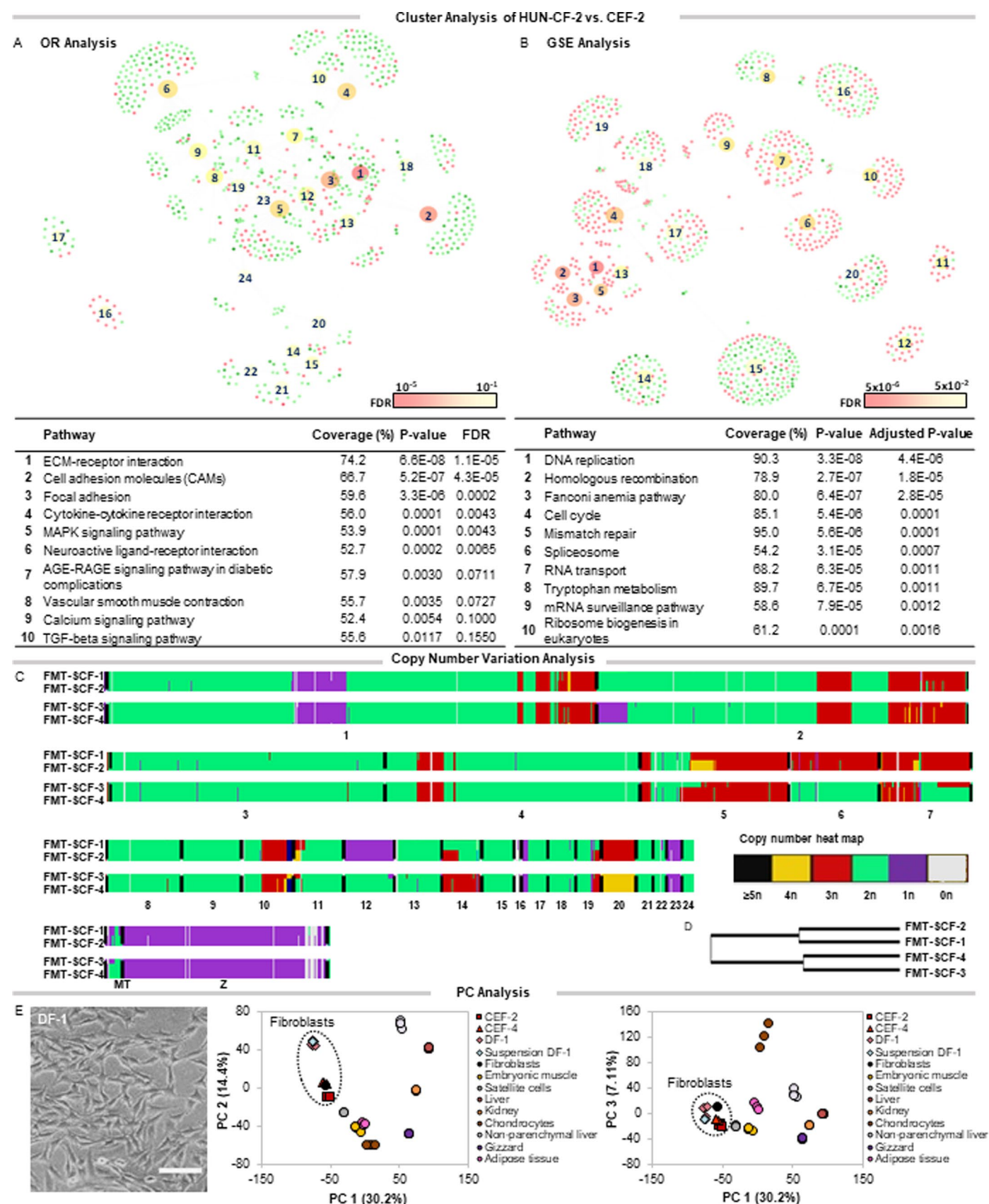
**Extended Data Fig. 1 | Spontaneous immortalization of chicken embryonic fibroblasts.** (A) Doubling time of primary cells from isolates 5 and 7. (B) Phase images of spontaneously immortalized chicken embryonic fibroblasts HUN-CF-2 and HUN-CF-4 compared to established DF-1 cell line (ATCC<sup>®</sup> CRL-12203). Scale

bar equals 100 μm. (C) Gene expression analysis of *TP53*, *PTEN*, and *ITGB3* in DF-1 compared with HUN-CF-2 and HUN-CF-4. (n = 3) Data are presented as means plus standard error of the mean.



**Extended Data Fig. 2 | Characterization of suspension-adapted chicken fibroblasts.** (A) Growth kinetics of FMT-SCF-2 in FBS-supplemented medium (DMEM10), commercial serum-free medium (UltraCULTURE™) and custom-made serum-free medium. (n = 3) (B) Species identity of cultured fibroblast origin was verified by PCR analysis. (C) Species identity of cultured fibroblast origin was verified by qRT-PCR using RapidFinder™ Chicken ID Kit validated kit.

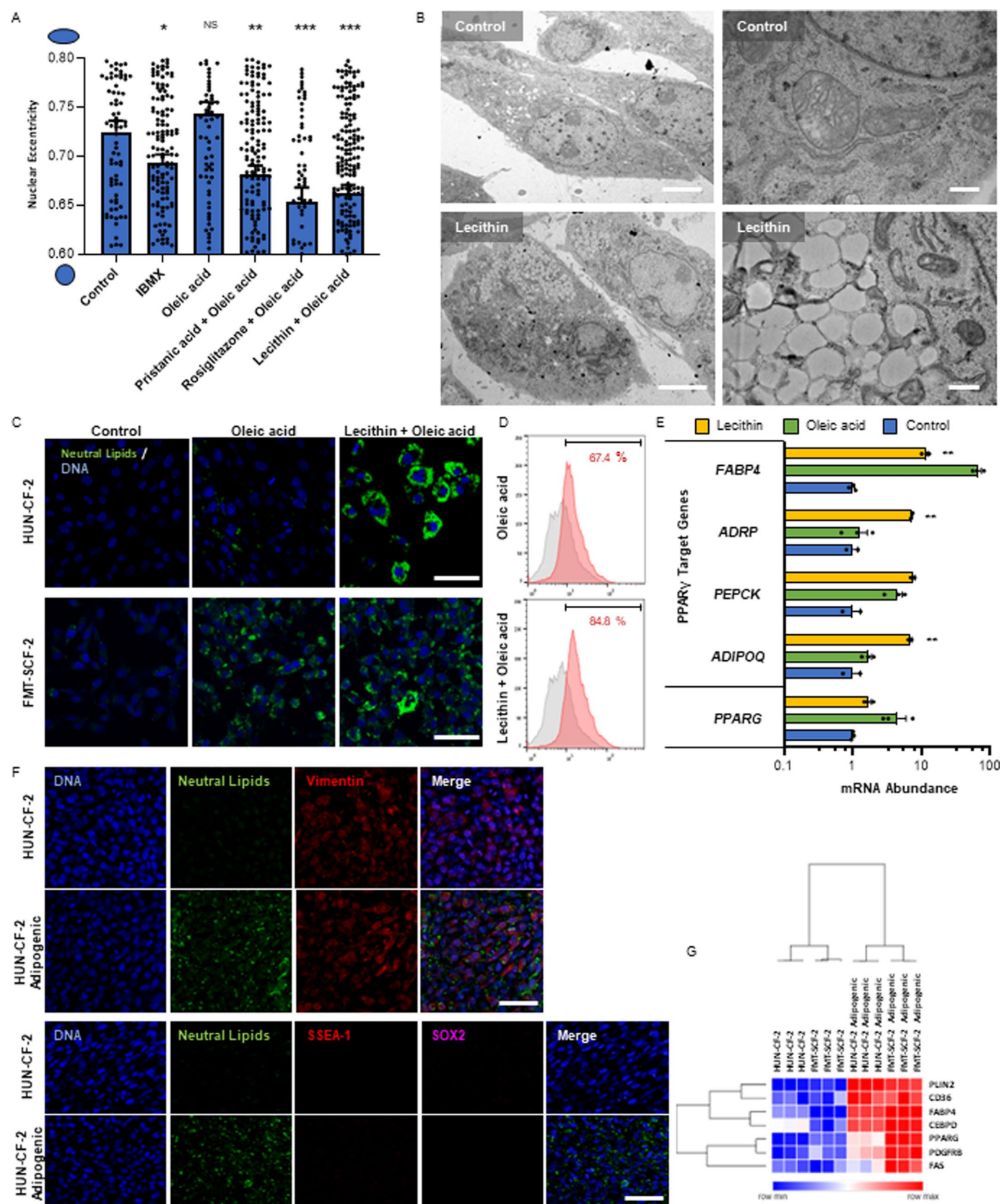
(D) Immunostaining of primary, immortalized adherent and suspension-adapted embryonic fibroblasts for Lamin A/C and Lamin B1. (E) Lamin A/C to Lamin B1 ratio in anchorage-independent fibroblasts (FMT-SCF-2) compared with primary adherent grown fibroblasts (CEF-2). Scale bar equals 20 μm. Data in panels A and E are presented as means plus standard error of the mean. Student's t test p values are labelled: \* p < 0.05, \*\* p < 0.01, \*\*\* p < 0.001.



Extended Data Fig. 3 | See next page for caption.

**Extended Data Fig. 3 | Sequencing analyses of immortalized and anchorage-independent chicken fibroblasts.** (A) K-mean clustering using Over-Representation (OR) Analysis of CEF-2 and HUN-CF-2. Full list of pathways (1-24) is provided in Supplementary Table 1 (S1A). Green: Downregulated genes, red: Upregulated genes. (B) K-mean clustering using Gene Set Enrichment (GSE) Analysis of CEF-2 and HUN-CF-2. Full list of pathways (1-20) is provided in Supplementary Table 1 (S1B). Green: Downregulated genes, red: Upregulated genes. (C) A heat map based on copy number variations (CNVs) of four immortalized chicken fibroblast lines, with FMT-SCF-1 and -2 derived from

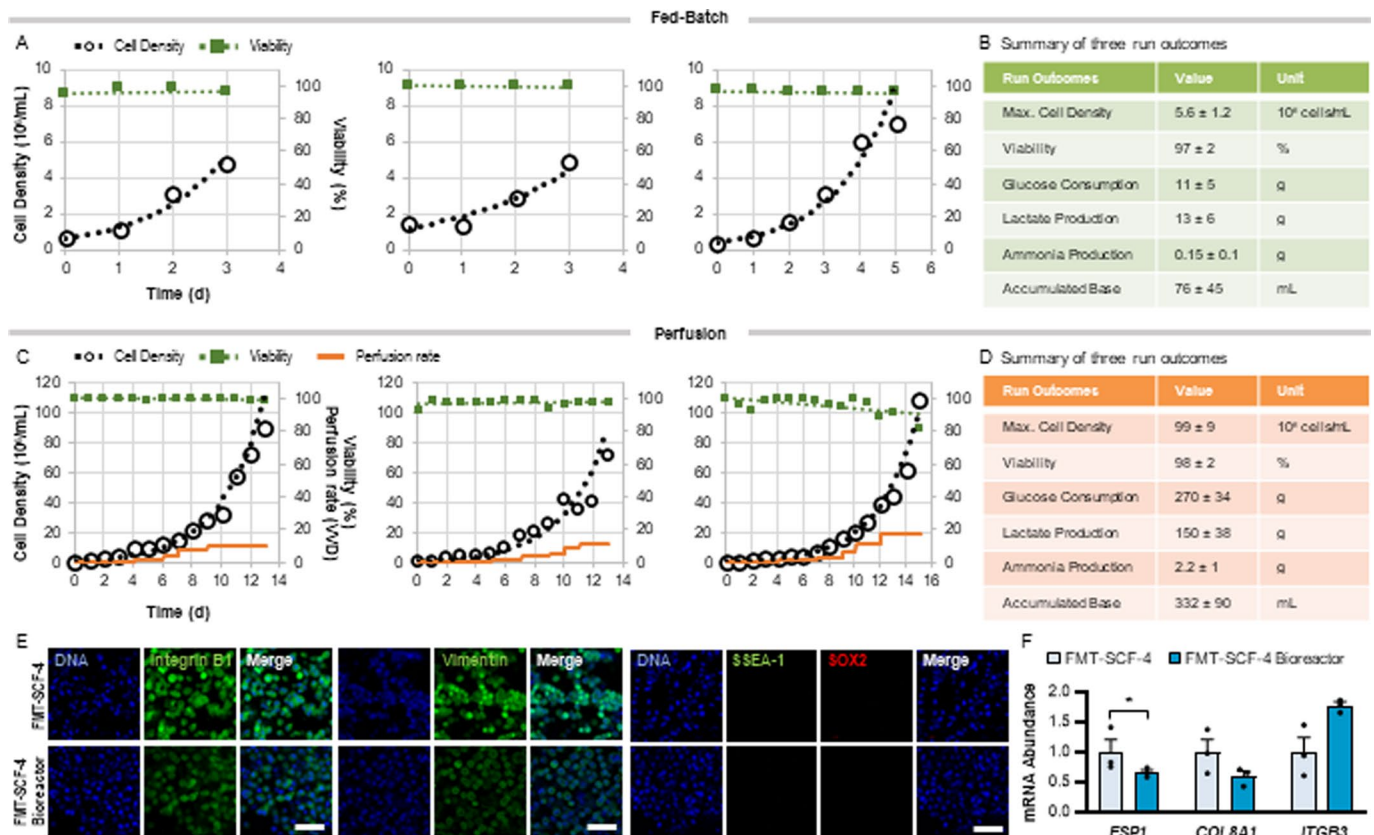
broiler Ross 308 and FMT-SCF-3 and -4 derived from Israeli Baladi chicken, respectively. Green: normal copy of genomic sequences (2n), purple: deletions of one copy (1n), turquoise: 2-copy deletion (0n). Red: (3n), orange: (4n) and black: (> 5 copies) mark duplication events. Boundaries between chromosomes are labelled black due to the repetitive sequence of the telomeres. (D) A phylogenetic tree of the four immortal chicken fibroblast lines based on similarities and differences in CNVs. (E) PCA of primary cells from broiler Ross 308 (CEF-2), Israeli Baladi (CEF-4), immortalized adherent and immortalized suspension lines of East Lansing (DF-1). Scale bar equals 100  $\mu$ m.



Extended Data Fig. 4 | See next page for caption.

**Extended Data Fig. 4 | Characterization of transdifferentiation potential in immortalized fibroblasts.** (A) Confocal image analysis of HUN-CF-2 cultured with adipogenesis-inducing agents pristanic acid, rosiglitazone, and lecithin. Nucleus rounded morphology and localizations as well as lipid droplet accumulation are indicative of immature adipocytes<sup>1</sup>. (B) TEM images showing cell shape and accumulation of fat in cells transdifferentiated with soy lecithin and oleic acid as compared to untreated control cells. Scale bars left to right, top to bottom equal 5  $\mu\text{m}$ , 500 nm, 5  $\mu\text{m}$ , and 500 nm, respectively. (C) Confocal images of HUN-CF-2 and FMT-SCF-2 following 7 days of transdifferentiation in medium containing oleic acid and oleic acid combined with soy lecithin. Scale

bars equal 50  $\mu\text{m}$ . (D) FACS analysis of FMT-SCF-2 cultured with oleic acid or lecithin and oleic acid. (n = 10,000 cells) (E) Gene expression analysis of *PPARG* and its target genes in FMT-SCF-2 treated with oleic acid. Fatty acid binding protein 4 (*FABP4*) upregulated in oleate stimulation possibly due to increased fatty acid trafficking<sup>2</sup>. (F) Confocal images of HUN-CF-2 following 7 days of transdifferentiation in adipogenic induction medium. Scale bars equal 50  $\mu\text{m}$ . (G) K-mean clustering heatmap of transdifferentiated adherent and suspension cultures with their respective input cell lines. (n = 3) Data in panels A and E are presented as means plus standard error of the mean. Student's t test p values are labelled: \*p < 0.05, \*\*p < 0.01, \*\*\*p < 0.001.



### Extended Data Fig. 5 | Characteristics of high density expanded biomass.

(A) Three independent fed-batch bioreactor runs showing cell density and viability in a culture of FMT-SCF-4. (B) Summary of the three fed-batch bioreactor outcomes. (C) Three independent continuously perfused bioreactor runs in a culture of FMT-SCF-4. (D) Summary of the three perfusion bioreactor run outcomes. (E) Confocal images of FMT-SCF-4 cells before and after bioreactor

expansion immunostained for Vimentin, Integrin B1, SOX2 and SSEA-1. Scale bars equal 50  $\mu$ m. (F) Gene expression analysis of fibroblast markers in FMT-SCF-4 cells before and after expansion in a bioreactor. (n = 3) Data are presented as means plus standard error of the mean. Student's t test p values are labelled: \*p < 0.05, \*\*p < 0.01, \*\*\*p < 0.001.





## Reporting Summary

Nature Research wishes to improve the reproducibility of the work that we publish. This form provides structure for consistency and transparency in reporting. For further information on Nature Research policies, see our [Editorial Policies](#) and the [Editorial Policy Checklist](#).

### Statistics

For all statistical analyses, confirm that the following items are present in the figure legend, table legend, main text, or Methods section.

n/a Confirmed

- |                                     |                                     |  |
|-------------------------------------|-------------------------------------|--|
| <input type="checkbox"/>            | <input checked="" type="checkbox"/> | The exact sample size ( $n$ ) for each experimental group/condition, given as a discrete number and unit of measurement  |
| <input type="checkbox"/>            | <input checked="" type="checkbox"/> | A statement on whether measurements were taken from distinct samples or whether the same sample was measured repeatedly  |
| <input type="checkbox"/>            | <input checked="" type="checkbox"/> | The statistical test(s) used AND whether they are one- or two-sided<br><i>Only common tests should be described solely by name; describe more complex techniques in the Methods section.</i>   |
| <input checked="" type="checkbox"/> | <input type="checkbox"/>            | A description of all covariates tested   |
| <input type="checkbox"/>            | <input checked="" type="checkbox"/> | A description of any assumptions or corrections, such as tests of normality and adjustment for multiple comparisons  |
| <input type="checkbox"/>            | <input checked="" type="checkbox"/> | A full description of the statistical parameters including central tendency (e.g. means) or other basic estimates (e.g. regression coefficient) AND variation (e.g. standard deviation) or associated estimates of uncertainty (e.g. confidence intervals) |
| <input checked="" type="checkbox"/> | <input type="checkbox"/>            | For null hypothesis testing, the test statistic (e.g. $F$ , $t$ , $r$ ) with confidence intervals, effect sizes, degrees of freedom and $P$ value noted<br><i>Give <math>P</math> values as exact values whenever suitable.</i>                            |
| <input checked="" type="checkbox"/> | <input type="checkbox"/>            | For Bayesian analysis, information on the choice of priors and Markov chain Monte Carlo settings   |
| <input checked="" type="checkbox"/> | <input type="checkbox"/>            | For hierarchical and complex designs, identification of the appropriate level for tests and full reporting of outcomes   |
| <input checked="" type="checkbox"/> | <input type="checkbox"/>            | Estimates of effect sizes (e.g. Cohen's $d$ , Pearson's $r$ ), indicating how they were calculated   |

*Our web collection on [statistics for biologists](#) contains articles on many of the points above.*

### Software and code

Policy information about [availability of computer code](#)

Data collection	ZEN Black/Blue 2012, Illumina HiSeqX , Cellaca MX High-throughput Automated Cell Counter integrated software, BioProfile® FLEX2 Automated Cell Culture Analyzer integrated software, Illumina's Novaseq S4, BD FACSDiva, QuantStudio, SCADA data acquisition, Tecnai 12 TEM 100kV operating software, TSL-EDAX operating software, NCBI GEO
Data analysis	MS Office 2016, RSEM, AneuFinder, R studio, DESeq2, Bowtie2, ggplot2 Morpheus, McGill's Network Analyst Tool, DAVID Informatics Resources, ImageJ2 Fiji, Cell Profiler, bwa mem, MarkDuplicate, haplotypeCaller, ENSEMBL Variant Effect Predictor, FATHMMcw, MuTect2, ANNOVAR, ZEN Black/Blue 2012, FlowJo, QuantStudio, STAR, TelSeq, Prism

For manuscripts utilizing custom algorithms or software that are central to the research but not yet described in published literature, software must be made available to editors and reviewers. We strongly encourage code deposition in a community repository (e.g. GitHub). See the Nature Research [guidelines for submitting code & software](#) for further information.

### Data

Policy information about [availability of data](#)

All manuscripts must include a [data availability statement](#). This statement should provide the following information, where applicable:

- Accession codes, unique identifiers, or web links for publicly available datasets
- A list of figures that have associated raw data
- A description of any restrictions on data availability

Sequencing data are available at NCBI GEO. The GEO accession number is GSE169291. All data generated or analyzed during this study are included in this published article (and its supplementary information files).

## Field-specific reporting

Please select the one below that is the best fit for your research. If you are not sure, read the appropriate sections before making your selection.

- Life sciences       Behavioural & social sciences       Ecological, evolutionary & environmental sciences

For a reference copy of the document with all sections, see [nature.com/documents/nr-reporting-summary-flat.pdf](https://www.nature.com/documents/nr-reporting-summary-flat.pdf)

## Life sciences study design

All studies must disclose on these points even when the disclosure is negative.

Sample size	Initial sample size per experiment was determined based on preliminary studies, and were different for different types of assays, as necessary to achieve statistical significance of data. Experiments were repeated multiple times in triplicate samples unless indicated otherwise. Images were analyzed from multiple fields (>5) and/or as single cells, low SEM was enough to establish a high level of statistical significance.
Data exclusions	No data exclusion was done on bulk quantifications and limited n quantification (qPCR, etc.). Multiple fields and other experiments with many technical repeats or measurements were assessed using Peirce's criterion ('Peirce' R Package) and outliers were removed for analysis. RNA-seq data was treated as described in the method section, based on previously established methods.
Replication	Experiments were repeated multiple times in triplicate technical repeats. Images were analyzed from multiple fields (>5) and/or as single cells, low SEM was enough to establish a high level of statistical significance.
Randomization	Treatments were allocated randomly within the same well plate the experiment was conducted in.
Blinding	Investigators providing specific analytical assessments and mass analysis were blinded to experimental group allocation.

## Reporting for specific materials, systems and methods

We require information from authors about some types of materials, experimental systems and methods used in many studies. Here, indicate whether each material, system or method listed is relevant to your study. If you are not sure if a list item applies to your research, read the appropriate section before selecting a response.

### Materials & experimental systems

- |                                     |   |
|-------------------------------------|---|
| n/a                                 | Involved in the study   |
| <input type="checkbox"/>            | <input checked="" type="checkbox"/> Antibodies                  |
| <input type="checkbox"/>            | <input checked="" type="checkbox"/> Eukaryotic cell lines       |
| <input checked="" type="checkbox"/> | <input type="checkbox"/> Palaeontology and archaeology          |
| <input type="checkbox"/>            | <input checked="" type="checkbox"/> Animals and other organisms |
| <input type="checkbox"/>            | <input checked="" type="checkbox"/> Human research participants |
| <input checked="" type="checkbox"/> | <input type="checkbox"/> Clinical data                          |
| <input checked="" type="checkbox"/> | <input type="checkbox"/> Dual use research of concern           |

### Methods

- |                                     |  |
|-------------------------------------|--|
| n/a                                 | Involved in the study                              |
| <input checked="" type="checkbox"/> | <input type="checkbox"/> ChIP-seq                  |
| <input type="checkbox"/>            | <input checked="" type="checkbox"/> Flow cytometry |
| <input checked="" type="checkbox"/> | <input type="checkbox"/> MRI-based neuroimaging    |

## Antibodies

### Antibodies used

Primary antibodies:  
 Rabbit Anti-Integrin beta 1 antibody AbCam ab183666  
 Rabbit Anti-Vimentin antibody [EPR3776] AbCam ab92547  
 Mouse Anti-Lamin A/C antibody (4C11) CellSignal mAB#4777  
 Rabbit Anti-Lamin B1 [EPR8985(B)] AbCam ab133741  
 Mouse Anti-SSEA-1 [MC-480] AbCam ab16285  
 Rabbit Anti-SOX2 AbCam ab97959  
 Secondary antibodies:  
 Alexa Fluor® 647 Donkey Anti-Mouse IgG (H+L) AbCam ab150111  
 Alexa Fluor® 488 AffiniPure Donkey Anti-Rabbit IgG (H+L) Jackson labs AB\_2313584  
 Alexa Fluor® 594 AffiniPure Donkey Anti-Mouse IgG (H+L) Jackson labs AB\_2340854  
 Alexa Fluor® 594 AffiniPure Donkey Anti-Rabbit IgG (H+L) Jackson labs AB\_2340621

### Validation

Validated on primary fibroblasts, based on component structure, morphology and localization

## Eukaryotic cell lines

Policy information about [cell lines](#)

Cell line source(s)	UMNSAH/DF-1 (ATCC® CRL-12203™), Hep G2 [HEPG2] (ATCC® HB-8065), HeLa (CRM-CCL-2™) were obtained from ATCC. The human hepatoma cell line (Huh7) was obtained from Creative Biolabs (Creative Biolabs, Shirley, NY, USA). Other cell lines were isolated in this study and described within.
Authentication	Cell lines from ATCC were validated by the source, and routinely authenticated by morphology. Other cell lines were authenticated routinely by morphology, species identification by PCR and qPCR.
Mycoplasma contamination	Cultures were routinely checked for infection, using PCR-based assay HY-MYCOPLASMA PCR KIT
Commonly misidentified lines (See <a href="#">ICLAC</a> register)	N/A

## Animals and other organisms

Policy information about [studies involving animals](#); [ARRIVE guidelines](#) recommended for reporting animal research

Laboratory animals	The study did not involve laboratory animals
Wild animals	The study did not involve wild animals
Field-collected samples	The study did not involve field collected samples
Ethics oversight	This study was reviewed and exempt by the institutional review board of the Hebrew University of Jerusalem, Israel.

Note that full information on the approval of the study protocol must also be provided in the manuscript.

## Human research participants

Policy information about [studies involving human research participants](#)

Population characteristics	Participants included multiple ethnic backgrounds. More detailed information is provided in the methods.
Recruitment	Participants were recruited by invitation.
Ethics oversight	The study was reviewed and approved by the Hebrew University of Jerusalem Institutional Review Board, Israel (#13092021).

Note that full information on the approval of the study protocol must also be provided in the manuscript.

## Flow Cytometry

### Plots

Confirm that:

- The axis labels state the marker and fluorochrome used (e.g. CD4-FITC).
- The axis scales are clearly visible. Include numbers along axes only for bottom left plot of group (a 'group' is an analysis of identical markers).
- All plots are contour plots with outliers or pseudocolor plots.
- A numerical value for number of cells or percentage (with statistics) is provided.

### Methodology

Sample preparation	SCF-2 anchorage-independent immortalized fibroblasts driven to transdifferentiate to adipocytes were stained with HCS LipidTOX™ neutral lipid stain and Hoechst 33258 (B2883, Sigma Aldrich) according to manufacturer's directions. Cells were washed 3 times and resuspended in FACS buffer containing phosphate buffer saline supplemented with calcium, magnesium, and 10% FBS.
Instrument	BD Biosciences FACS Aria III cell sorter (San Jose, CA)
Software	BD FACSDiva, FlowJo
Cell population abundance	Rosiglitazone induced intracellular accumulation of lipid droplets in 64% of the population following 7 days of exposure. Pristanic acid induced a more homogenous accumulation of lipid droplets in 93% of the population. Phosphatidylcholine (lecithin) exposure induced a robust accumulation of lipid droplets in 84% of the cell population. The untreated population is referred to as "negative control" and exhibited a lipid droplet accumulation of 30.8% while IBMX/Dexamethasone showed 34.4%.

Gating strategy

Gating was determined based on preliminary experiments performed on non treated cells (referred to as "control").

Tick this box to confirm that a figure exemplifying the gating strategy is provided in the Supplementary Information.